CALET results on cosmic-ray nuclei and electrons after 9 years of observations on the ISS

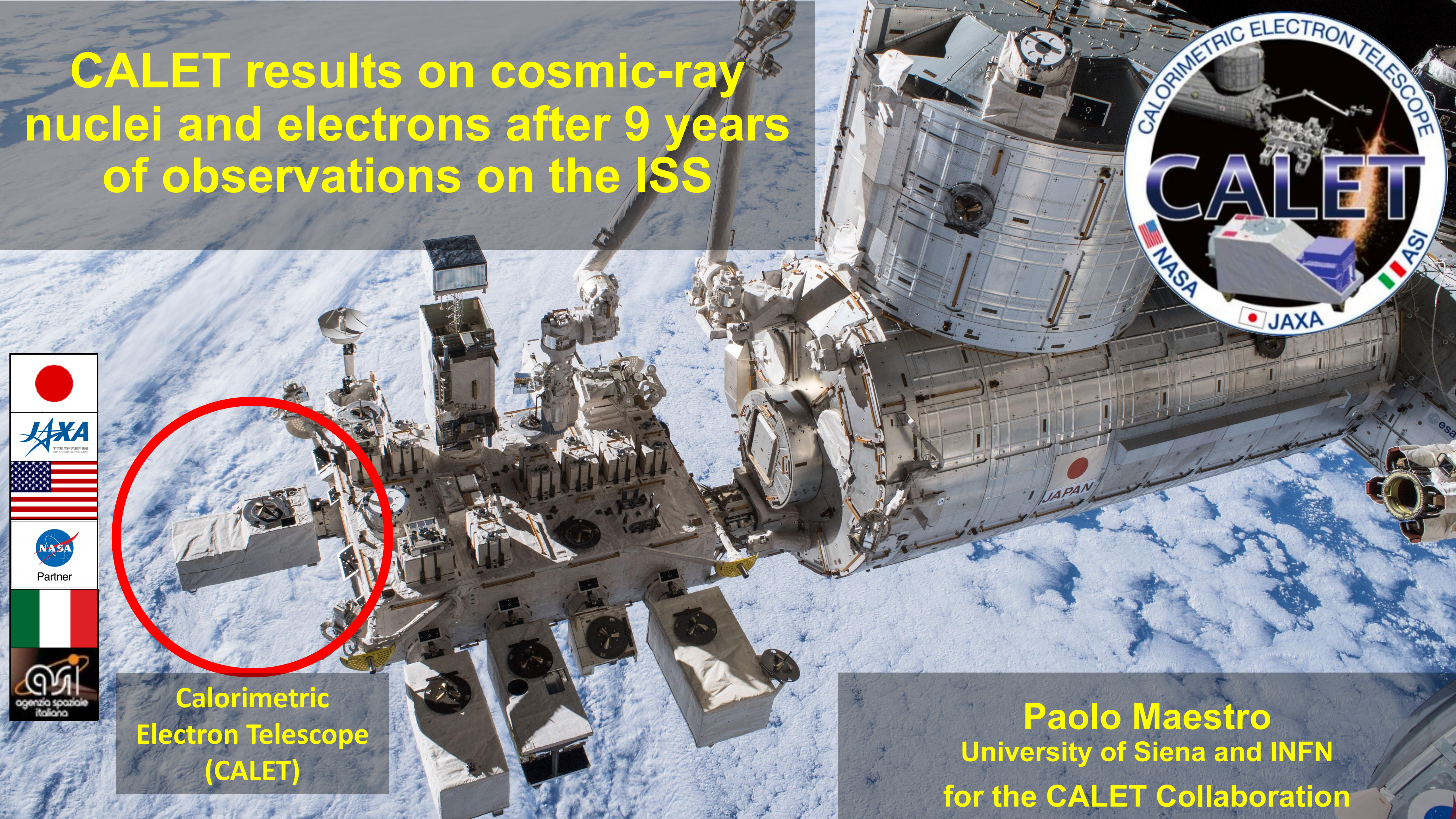

Calorimetric Electron Telescope (CALET)

Paolo Maestro
University of Siena and INFN
for the CALET Collaboration

The CALET Collaboration

O. Adriani,[1,2] Y. Akaike,[3,4] K. Asano,[5] Y. Asaoka,[5] E. Berti,[2,6] G. Bigongiari,[7,8] W. R. Binns,[9] M. Bongi,[1,2] P. Brogi,[7,8] A. Bruno,[10] N. Cannady,[11,12,13] G. Castellini,[6] C. Checchia,[7,8] M. L. Cherry,[14] G. Collazuol,[15,16] G. A. de Nolfo,[10] K. Ebisawa,[17] A. W. Ficklin,[14] H. Fuke,[17] S. Gonzi,[1,2,6] T. G. Guzik,[14] T. Hams,[11] K. Hibino,[18] M. Ichimura,[19] W. Ishizaki,[5] M. H. Israel,[9] K. Kasahara,[20] J. Kataoka,[21] R. Kataoka,[22] Y. Katayose,[23] C. Kato,[24] N. Kawanaka,[25,26] Y. Kawakubo,[14] K. Kobayashi,[3,4] K. Kohri,[26,27] H. S. Krawczynski,[9] J. F. Krizmanic,[12] P. Maestro,[7,8] P. S. Marrocchesi,[7,8] A. M. Messineo,[8,28] J. W. Mitchell,[12] S. Miyake,[29] A. A. Moiseev,[12,13,30] M. Mori,[31] N. Mori,[2] H. M. Motz,[32] K. Munakata,[24] S. Nakahira,[17] J. Nishimura,[17] M. Negro,[14] S. Okuno,[18] J. F. Ormes,[33] S. Ozawa,[34] L. Pacini,[2,6] P. Papini,[2] B. F. Rauch,[9] S. B. Ricciarini,[2,6] K. Sakai,[11,12,13] T. Sakamoto,[35] M. Sasaki,[12,13,30] Y. Shimizu,[18] A. Shiomi,[36] P. Spillantini,[1] F. Stolzi,[7,8] S. Sugita,[35] A. Sulaj,[7,8] M. Takita,[5] T. Tamura,[18] T. Terasawa,[5] S. Torii,[3] Y. Tsunesada,[37,38] Y. Uchihori,[39] E. Vannuccini,[2] J. P. Wefel,[14] K. Yamaoka,[40] S. Yanagita,[41] A. Yoshida,[35] K. Yoshida,[20] W. V. Zober[9]

1) University of Florence, Italy
2) INFN Sezione di Firenze, Italy
3) RISE, Waseda University, Japan
4) JEM Utiliziation Center, JAXA, Japan
5) ICRR, University of Tokyo, Japan
6) IFAC, CNR, Italy
7) University of Siena, Italy
8) INFN Sezione di Pisa, Italy
9) Washington University in St. Louis, USA
10) Heliospheric Physics Laboratory, NASA GSFC, USA
11) University of Maryland, Baltimore County, USA
12) Astroparticle Physics Laboratory, NASA GSFC, USA
13) CRESST II, NASA GSFC, USA
14) Louisiana State University, USA
15) University of Padova, Italy
16) INFN Sezione di Padova, Italy
17) ISAS, JAXA, Japan
18) Kanagawa University, Japan
19) Hirosaki University, Japan
20) Shibaura Institute of Technology, Japan
21) ASE, Waseda University, Japan
22) NIPR, Japan
23) Yokohama National University, Japan
24) Shinshu University, Japan
25) Tokyo Metropolitan University
26) NAO, Japan
27) IPNS, KEK, Japan
28) University of Pisa, Italy
29) KOSEN, NIT, Japan
30) University of Maryland, College Park, USA
31) Ritsumeikan University, Japan
32) GCSE, Waseda University, Japan
33) University of Denver, USA
34) NICT, Japan
35) Aoyama Gakuin University, Japan
36) Nihon University, Japan
37) Osaka Metropolitan University, Japan
38) NITEP, Osaka Metropolitan University, Japan
39) QST, Japan
40) Nagoya University, Japan
41) Ibaraki University, Japan

PI: Japan
Co-PI: Italy
Co-PI: USA

CALET payload

Launched on Aug. 19th 2015 on the Japanese H2-B rocket
Emplaced on JEM-EF port#9
On Aug. 25th 2015

Continuous and stable operations from Oct. 13th 2015

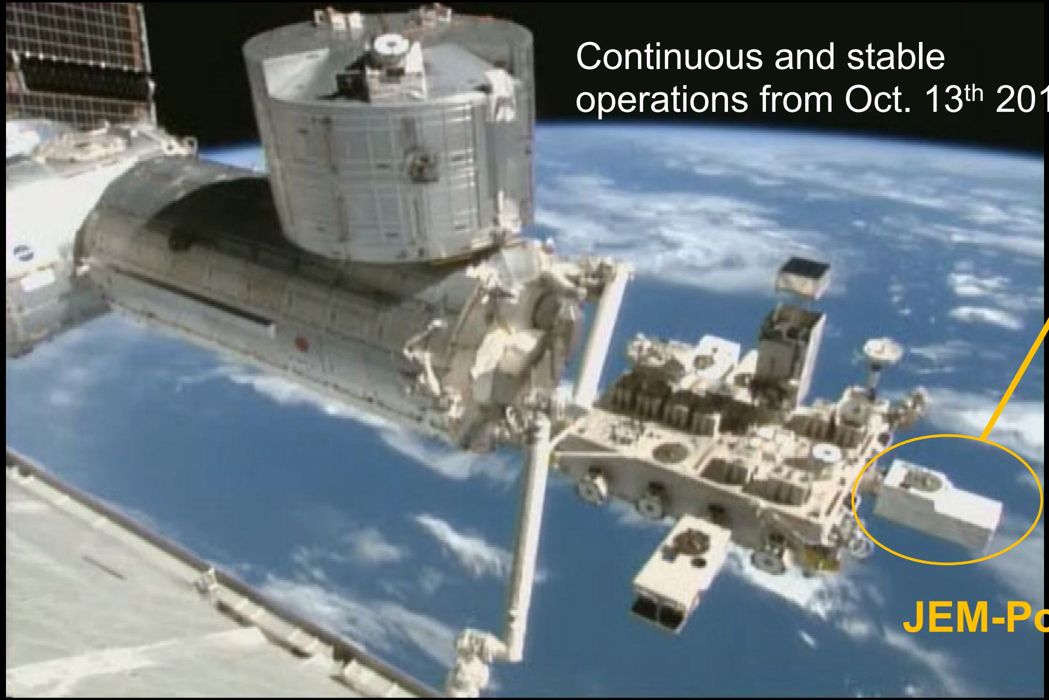

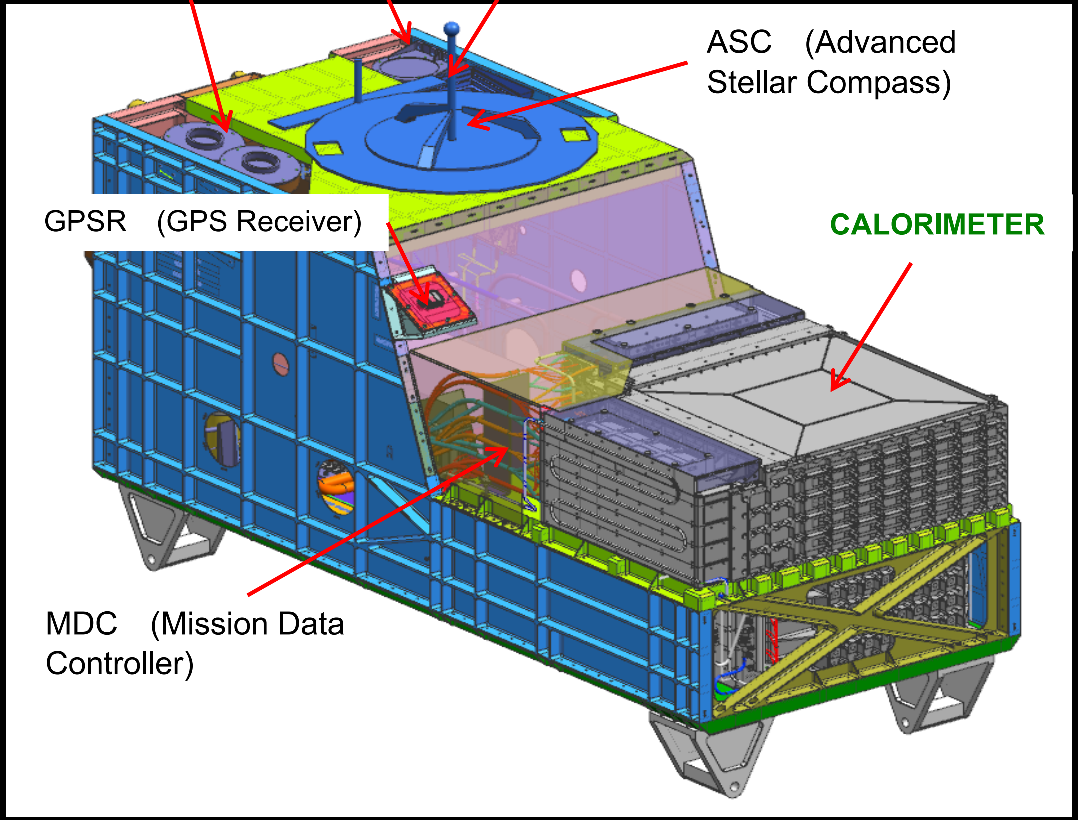

- Mass: 612.8 kg
- JEM Standard Payload Size
  1850 mm (L) × 800 mm (W) × 1000 mm (H)
- Power Consumption: 507 W (max)
- Telemetry: Medium (Low) 600 (50) kbps (6.5GB/day)

CALET Calorimeter

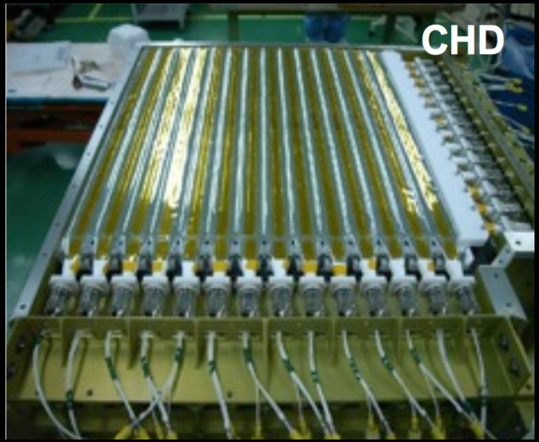

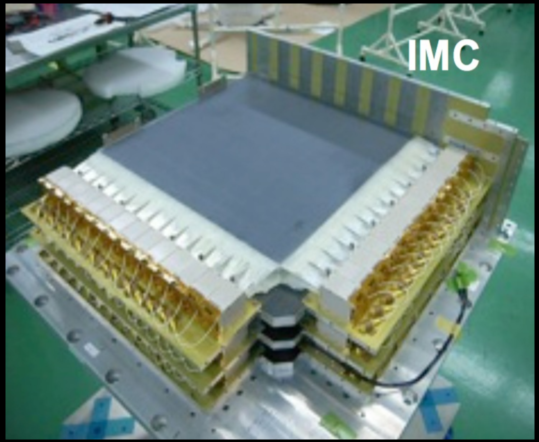

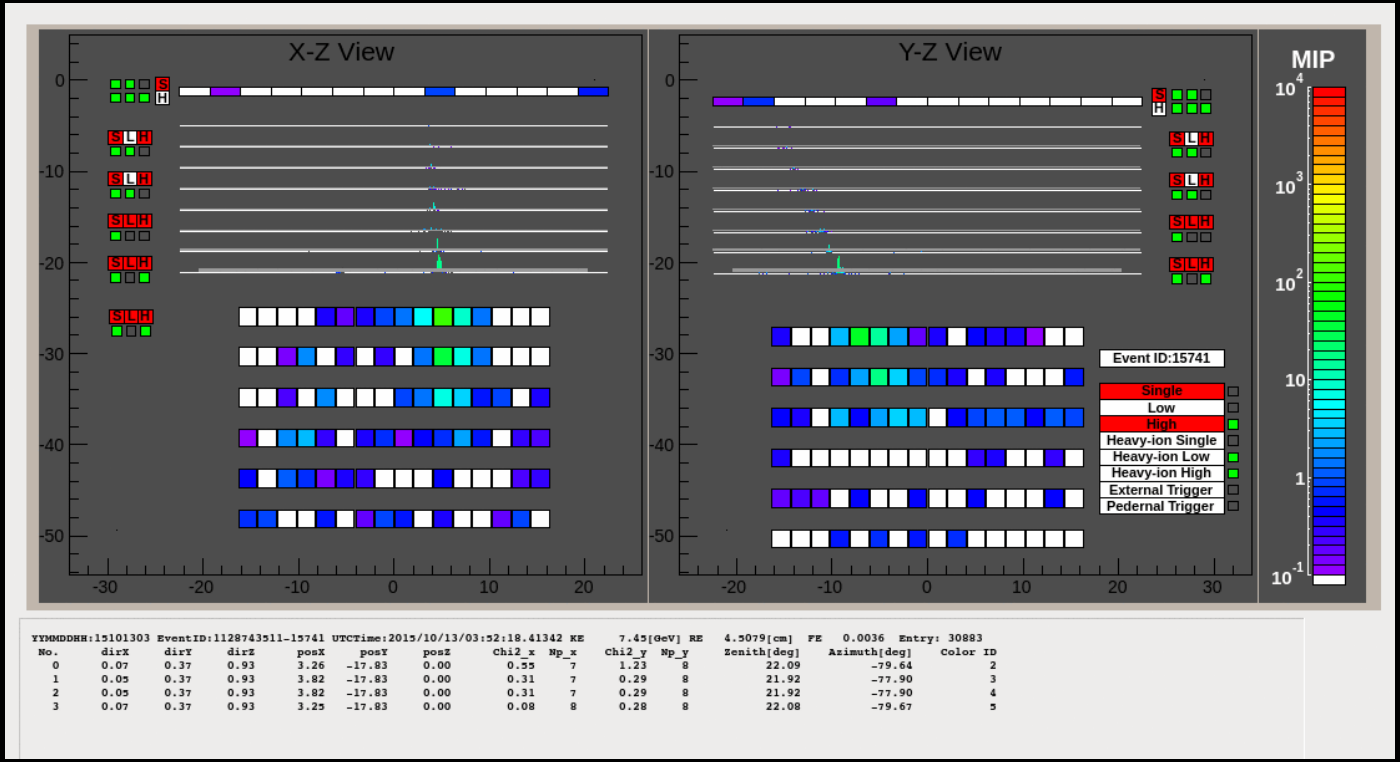

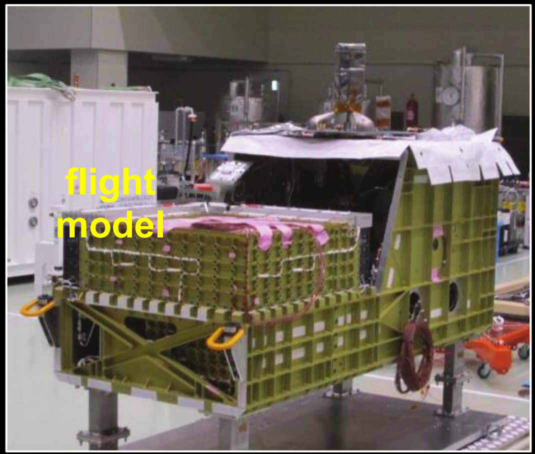

CHD **Charge Detector**	2 layers x 14 plastic scintillating paddles **single element charge ID** from p to Fe and up to Z = 40 charge resolution ~0.1-0.3 e	PMT+CSA
IMC **Imaging Calorimeter**	Scifi + 7 W absorbers: 3 X_0 at normal incidence 8 x 2 x 448 plastic scifi (1mm^2) readout individually **Tracking** (~0.1° angular resolution) + **Shower imaging**	64 MAPMT+ ASIC
TASC **Total Absorption Calorimeter**	Total thickness 27 $X_{0,}$ 1.2 λ_I 6 x 2 x 16 lead tungstate ($PbWO_4$) logs **Energy res.**: ~2% (>10 GeV) for e,γ ~30% for p,nuclei **e/p separation**: ~10^5	APD/PD + CSA PMT+CSA **Dynamic range:10^6**

CALET scientific objectives

Scientific Objectives	Observable Quantity	Energy Range
Cosmic-ray origin and acceleration	Electron spectrum	1 GeV – 20 TeV
	Elemental spectra	10 GeV – 1 PeV
	Ultra-heavy abundances	> 600 MeV/n
	Gamma rays (diffuse & point source)	1 GeV – 1 TeV
Galactic CR propagation	B/C and sub-Fe/Fe ratios	Up to some TeV/n
Nearby CR sources	Electron spectrum	100 GeV – 20 TeV
Dark matter	Signatures in electron/gamma spectra	100 GeV – 20 TeV
Solar physics	Electron flux	1 GeV – 10 GeV
Gamma-ray transients, GW counterparts	LE gamma rays and X-rays	7 keV – 20 MeV

TASC calibration

Y. Asaoka et al. (CALET Collaboration)
Astropart. Phys. 91 (2017) 1

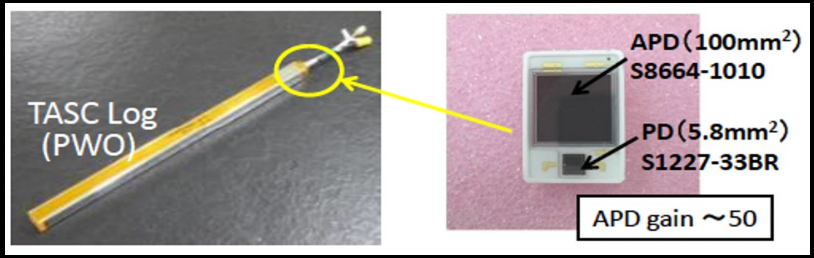

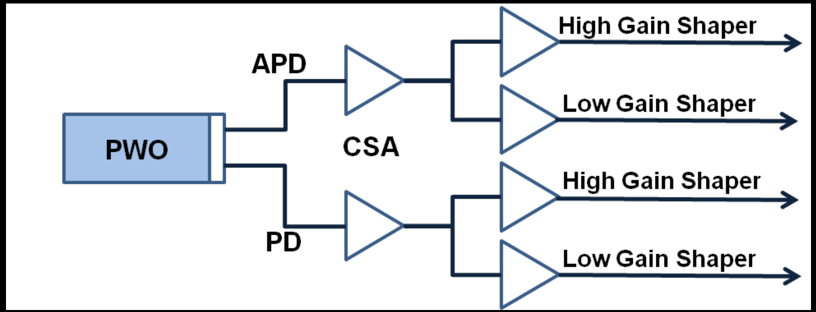

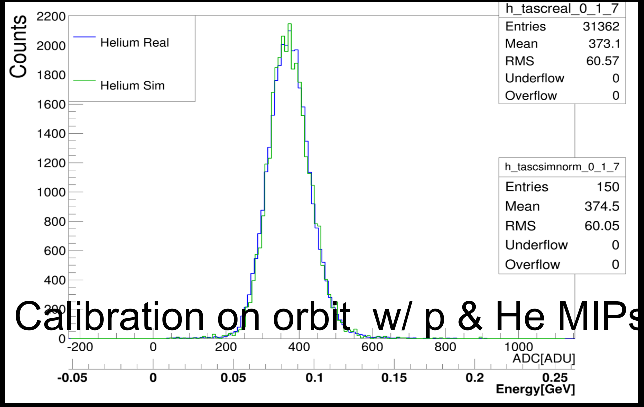

Calibration on orbit w/ p & He MIPs

Distribution of MIP's in all channels

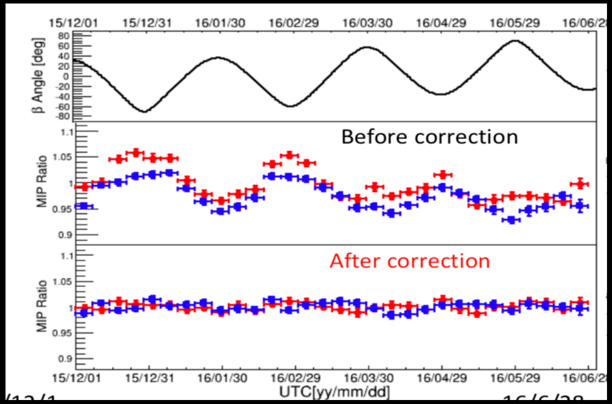

Corrections for position, temperature, latitude (due to rigidity) dependence

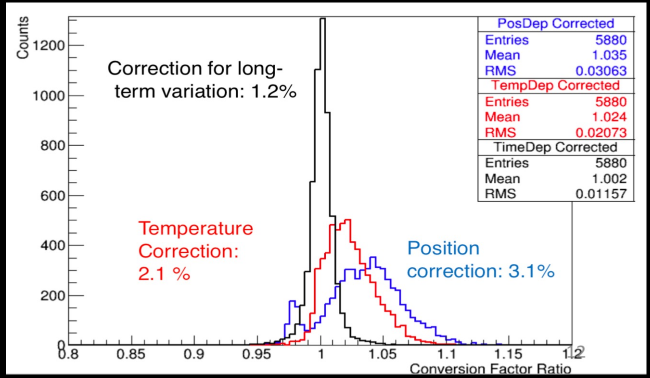

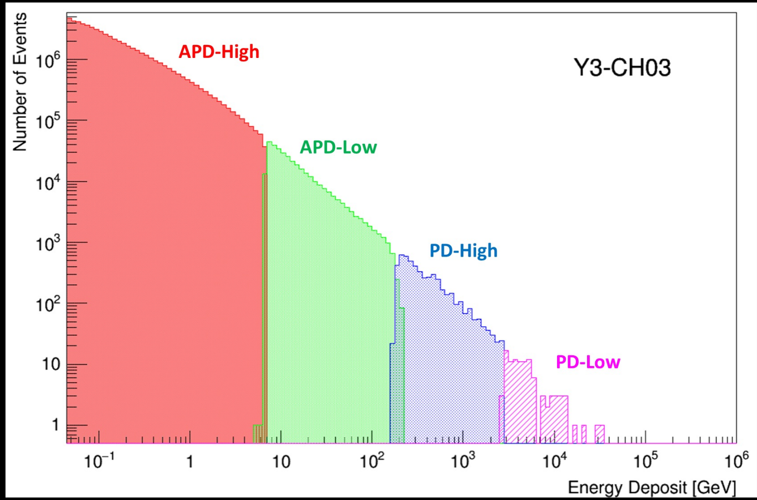

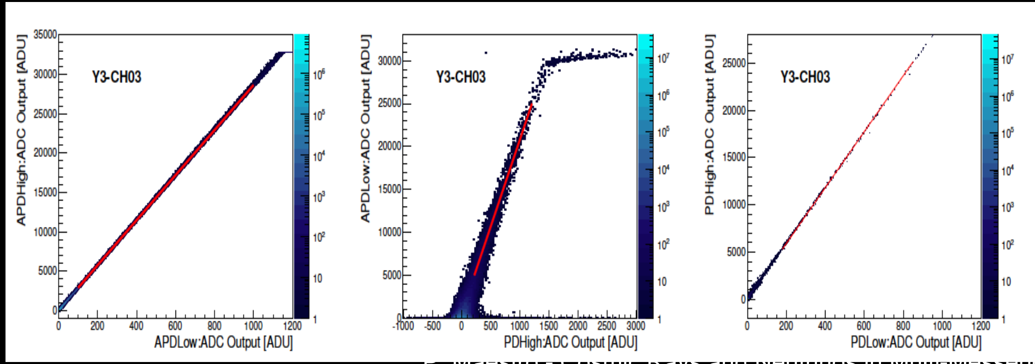

Gain ranges calibrated by UV laser irradiation on ground.
Correlation of gain ranges calibrated in-flight

Energy distribution in one PWO log.
Dynamic range of each channel: 1 - 10^6 MIP

Examples of CALET event candidates

Electron, E=3.05 TeV

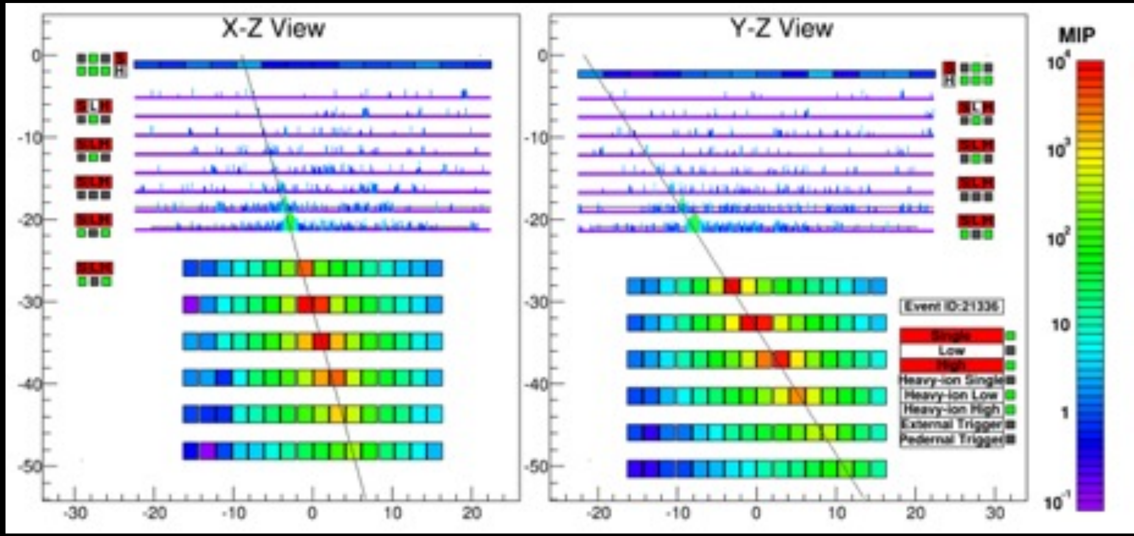

Proton, E_{TASC}=2.89 TeV

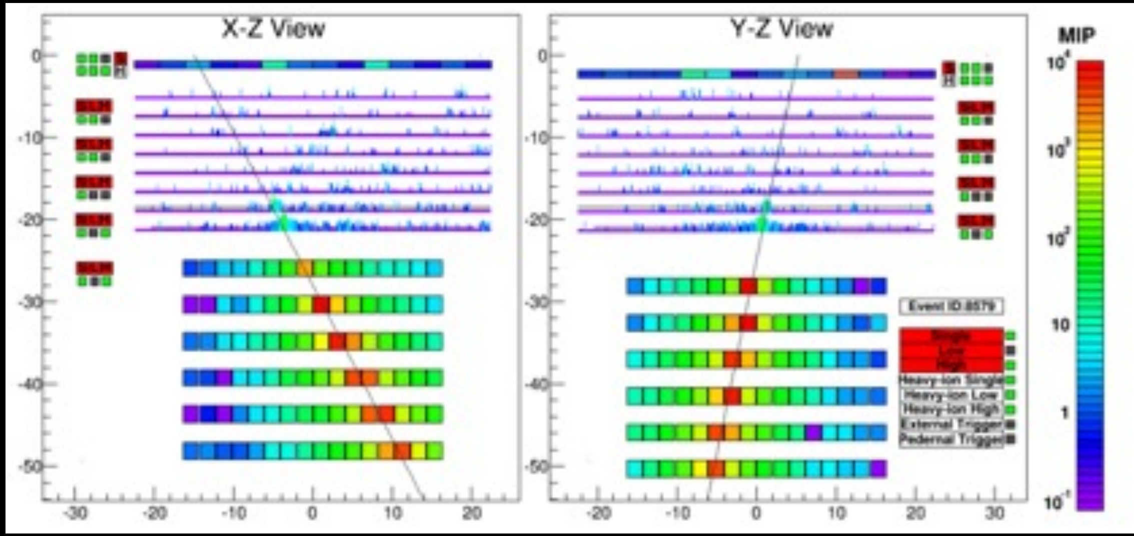

Gamma-ray, E=44.3 GeV

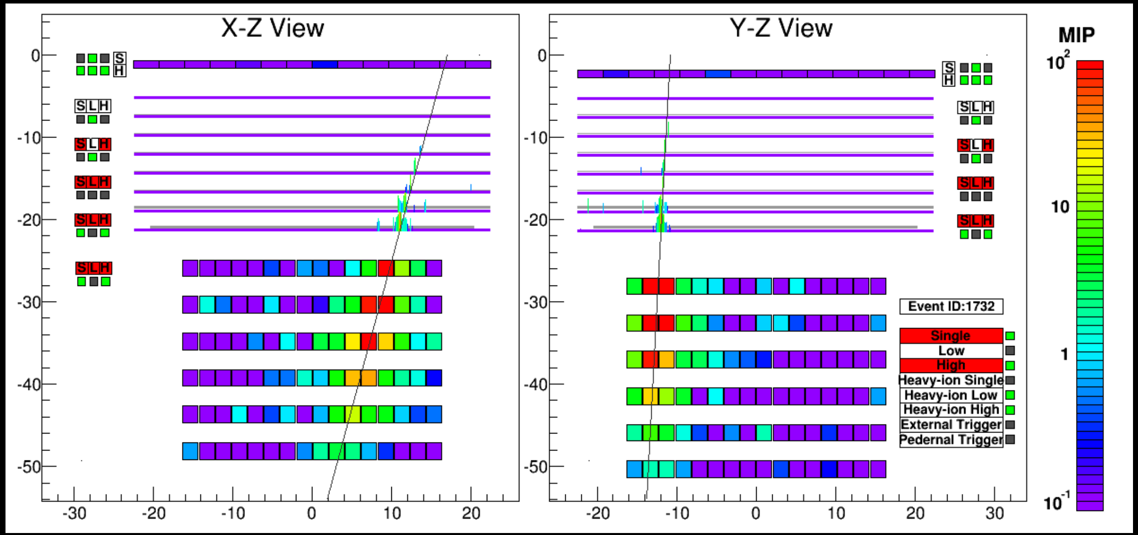

Iron, E_{TASC} =9.3 TeV

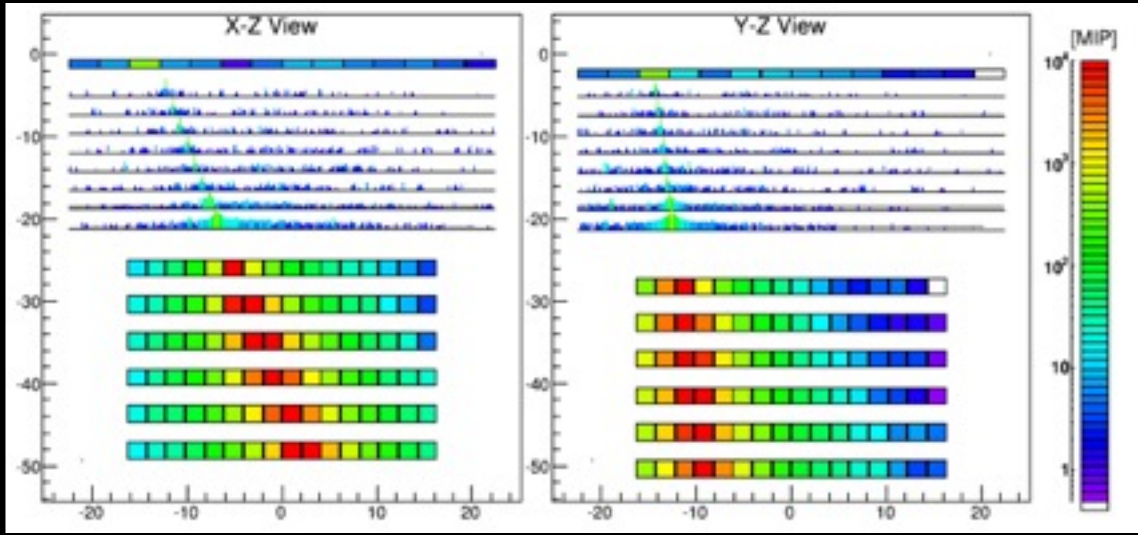

Energy measurement: energy scale and resolution

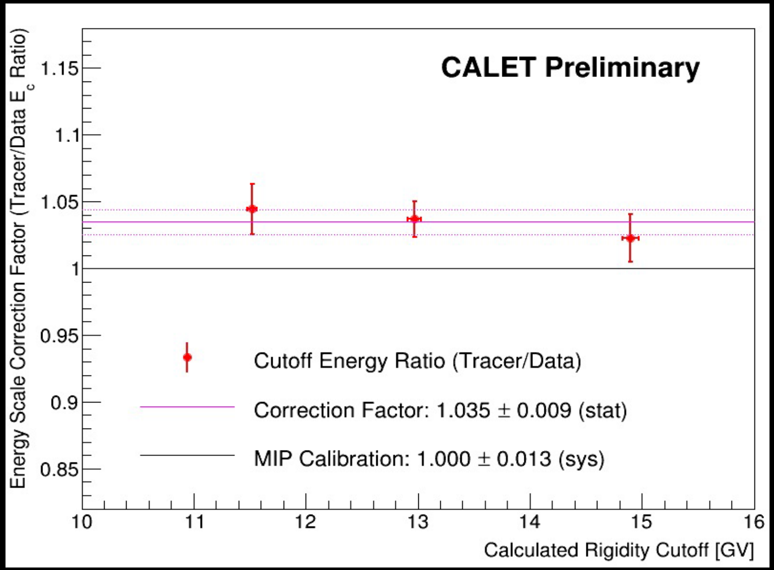

ELECTRONS

Beam calibration at CERN-SPS + rigidity cutoff

Energy resolution: < 2% above 20 GeV with both TASC and IMC including calibration errors

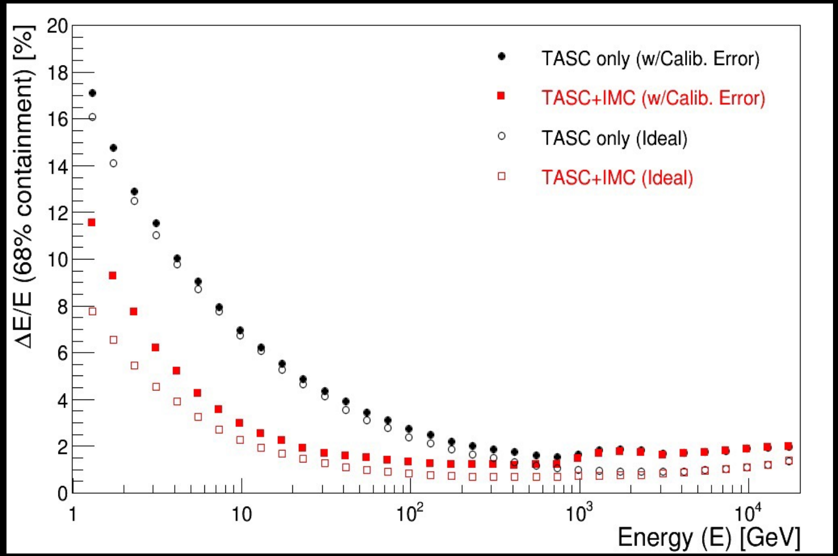

HADRONS

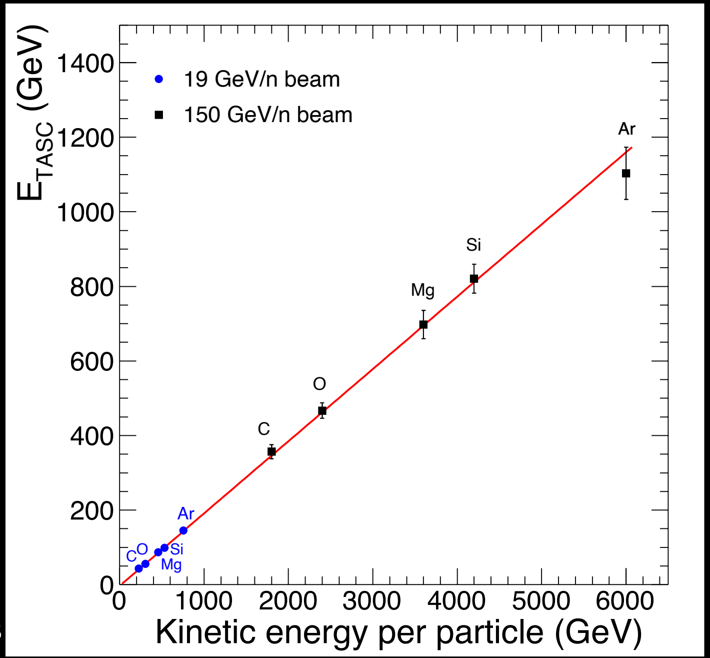

Beam calibration at CERN-SPS with ion fragments from primary Ar beam at 13, 19 150 GeV/n

Linearity assessed up to ~6 TeV
Fraction of particle energy released in TASC is ~20%

Energy resolution ~30%

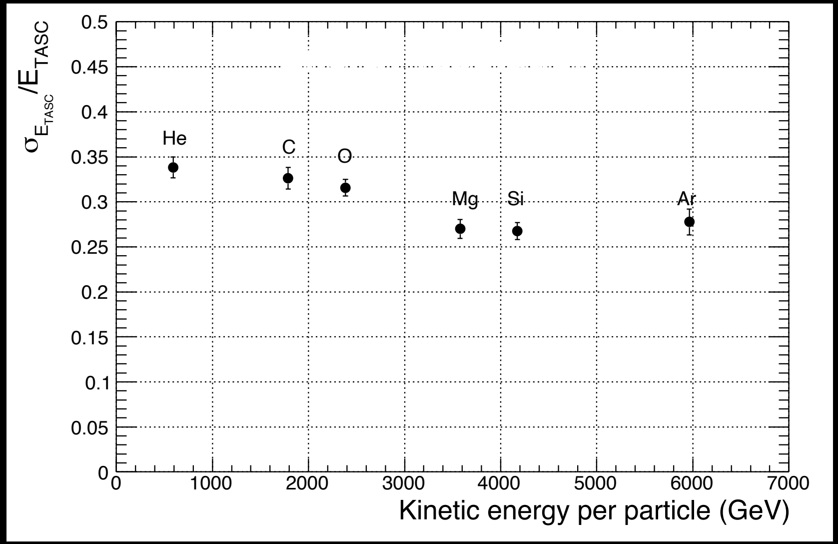

CALET Orbital Operations

Geometrical Factor:

- 1040 cm^2 sr for electrons, light nuclei
- 1000 cm^2 sr for gamma-rays
- 4000 cm^2sr for ultra-heavy nuclei

High-energy trigger (> 10 GeV) statistics:

- Orbital operations **>3200 days**
- Live time fraction **～ 86%**
- Exposure of HE trigger **～300 m^2 sr day**

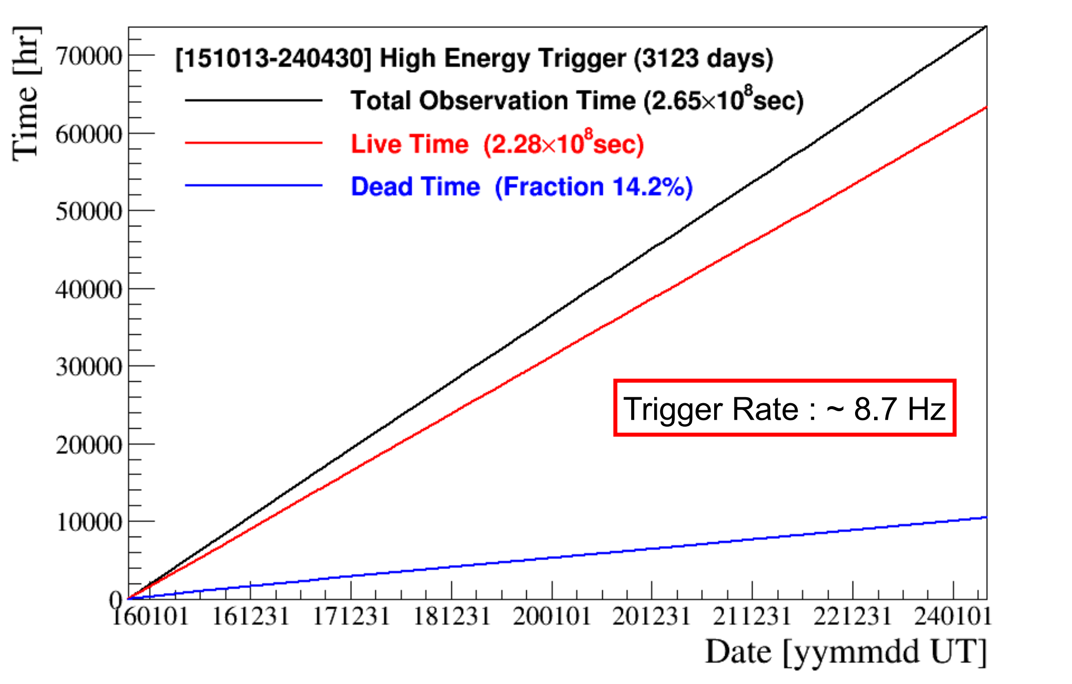

Energy deposit (in TASC) spectrum: 1 GeV-1 PeV

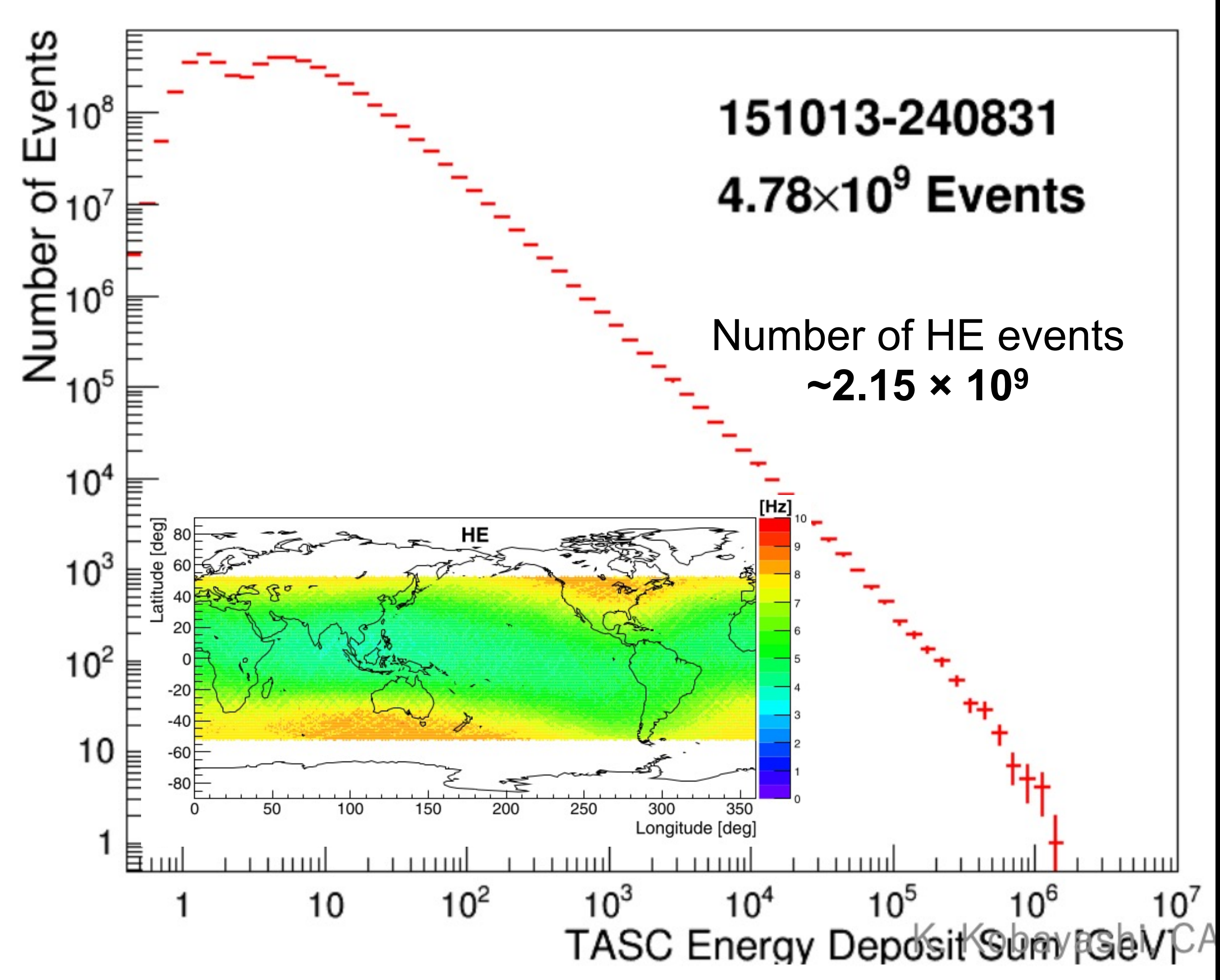

Cosmic-ray all electron spectrum

PRL 131 191001 (2023)
ICRC2023 Pos 071

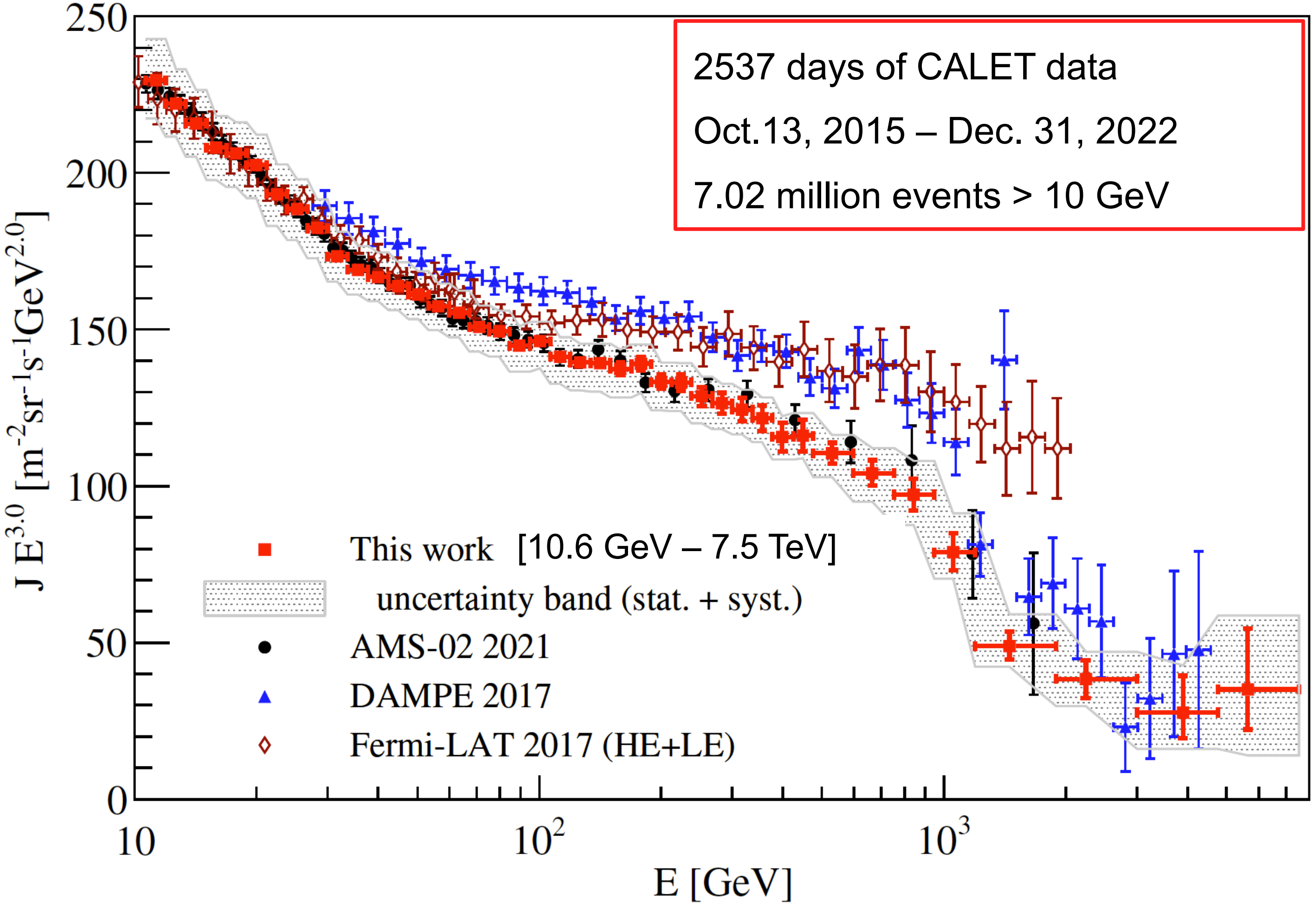

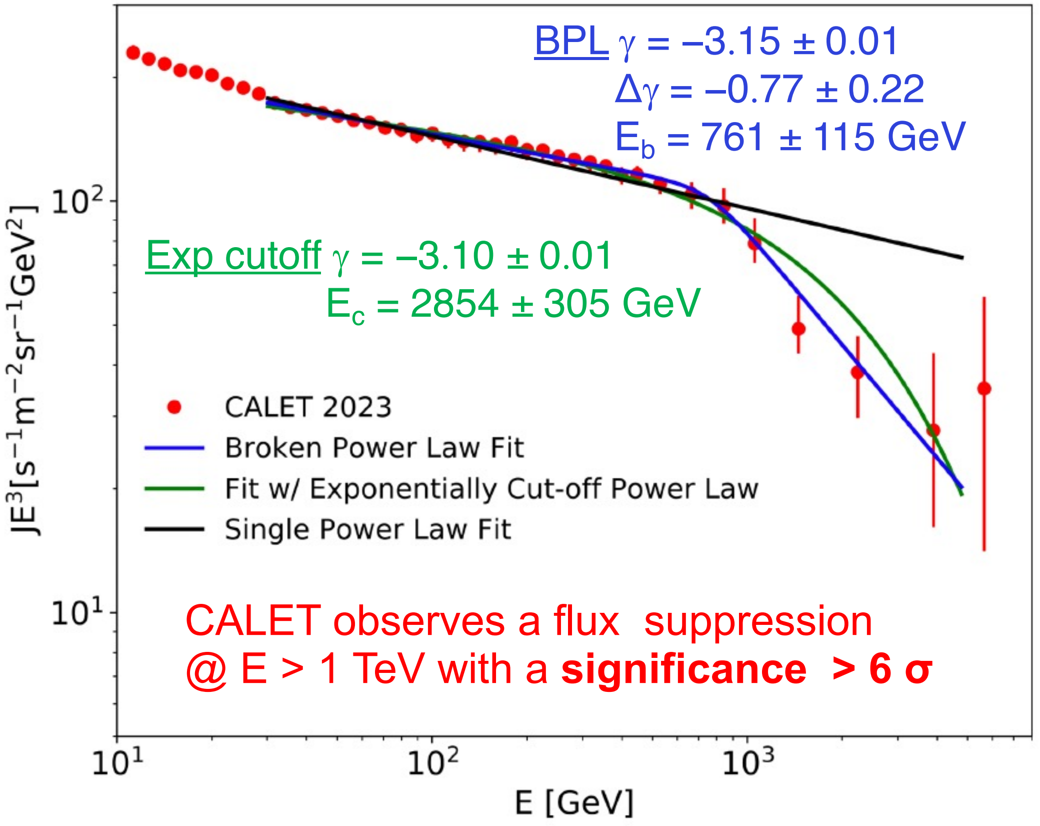

Continued observation has reduced statistical and systematic errors in the all-electron spectrum.
Systematic discrepancy between CALET/AMS-02 and DAMPE/Fermi-LAT persists beyond tabulated error.

Softening of the spectrum is above 1 TeV

Only nearby (<~1 kpc) and young (<~10^5 yr) sources can contribute to electron flux @ E>1 TeV

TeV electrons

PRL 131 191001 (2023)
ICRC2023 Pos 062, 067

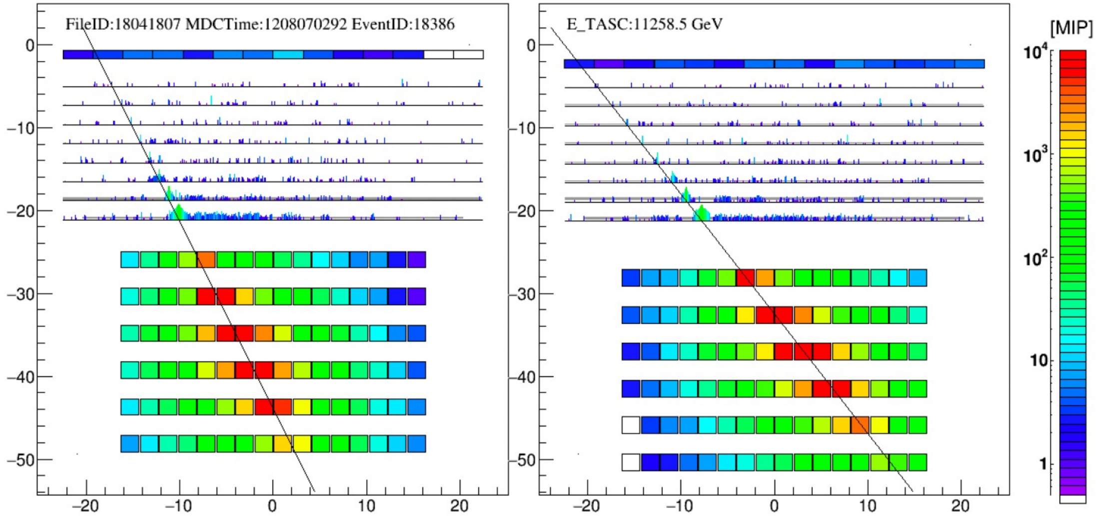

Nearby accelerators could leave observable features in the spectrum in the TeV region.

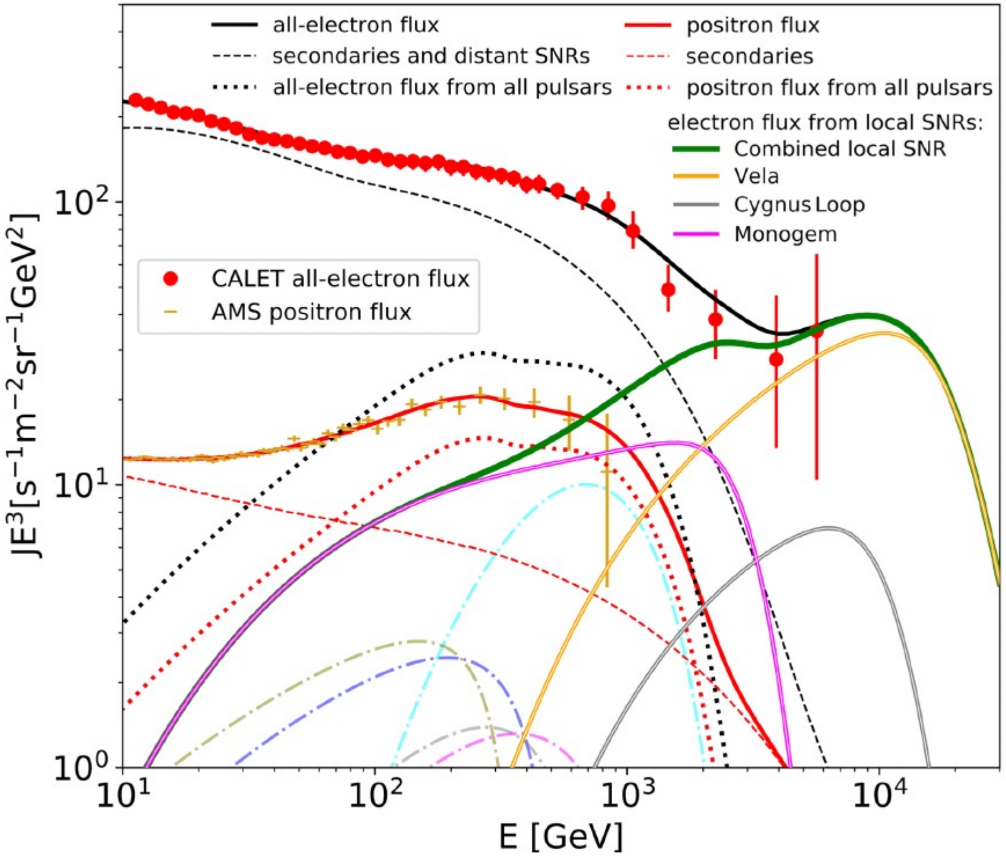

Advanced analysis is going on for electron identification @ E > 5 TeV.

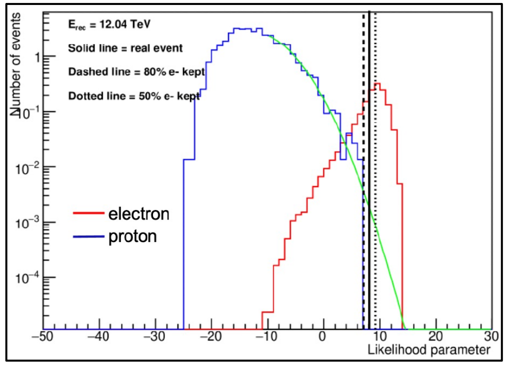

The observed numbers of electron candidates obtained by the event-by-event analysis are 9 (4) above 4.8 TeV (7.5 TeV), compatible with the expected contribution from the nearby SNRs

Cosmic-ray proton spectrum

PRL 129 101102 (2022)
ICRC2023 Pos 092

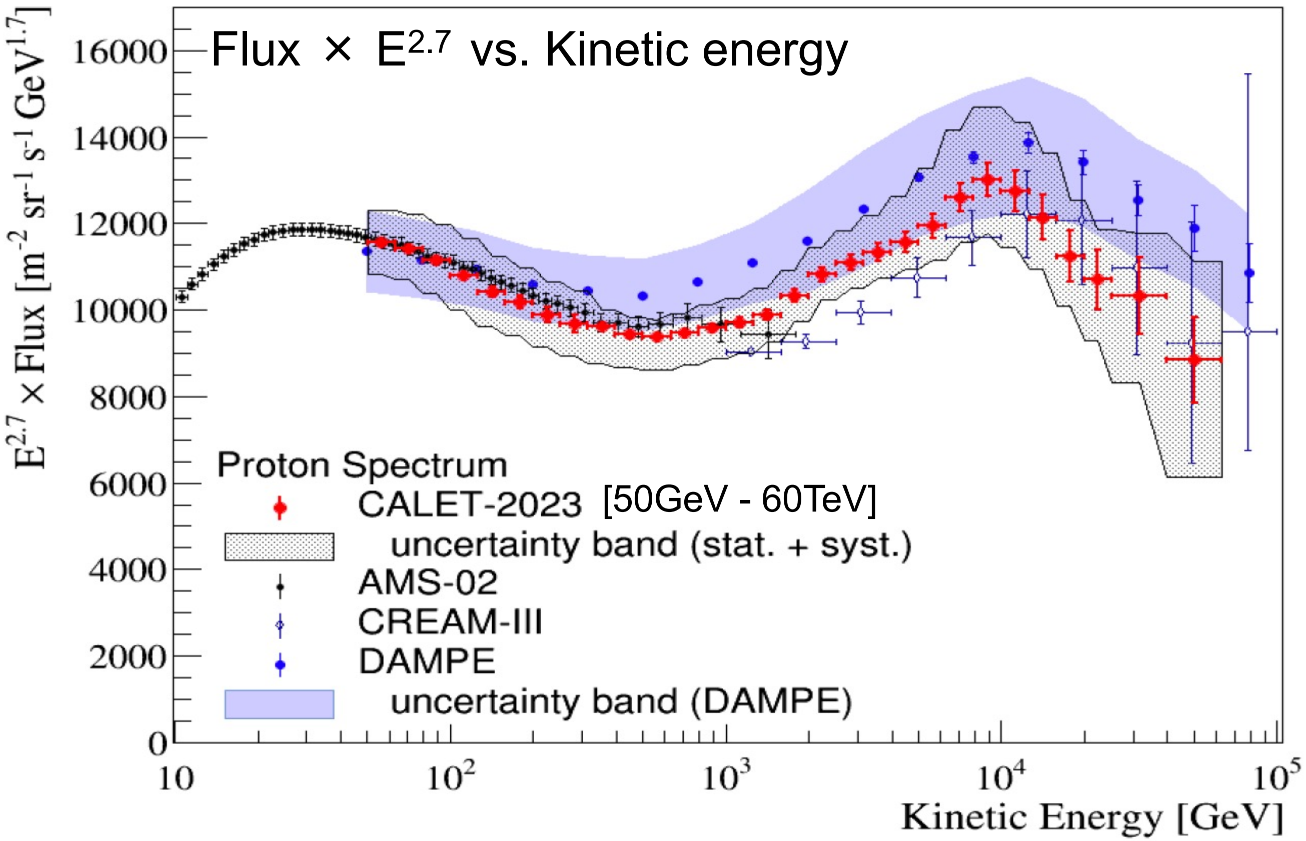

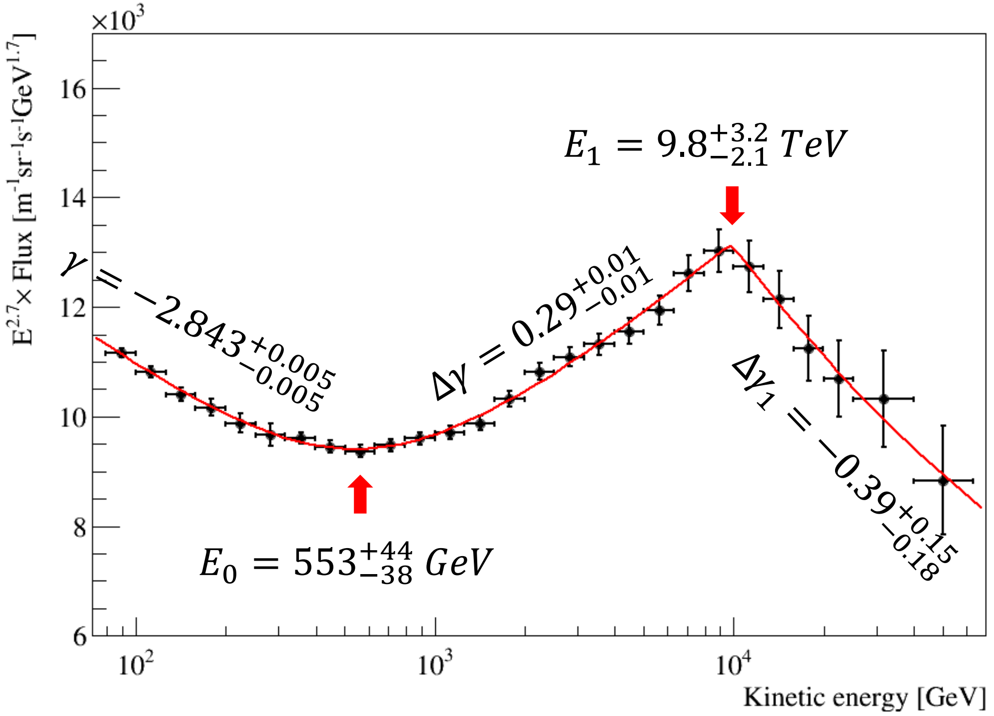

Spectral index energy dependence

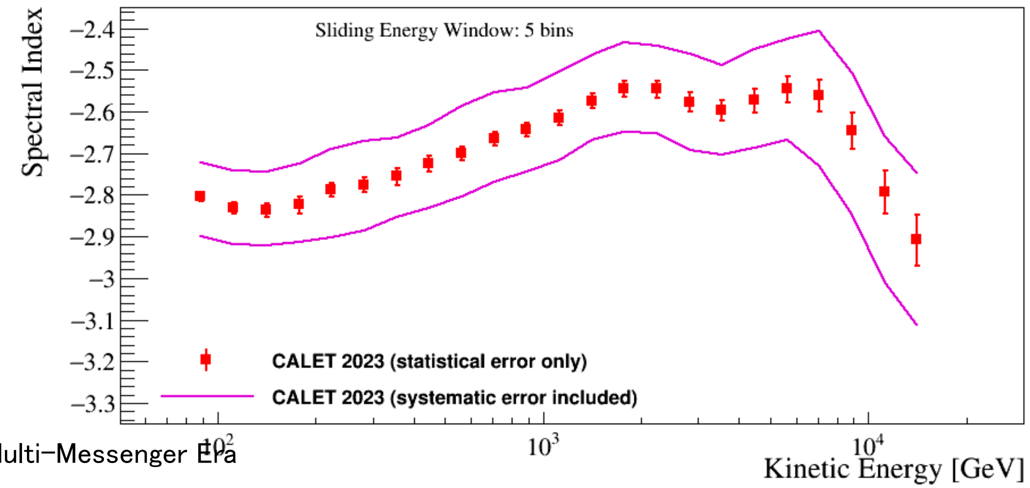

Double Power Law Function: HARDENING SOFTENING

$$\Phi(E) = C\left(\frac{E}{\mathrm{GeV}}\right)^{\gamma}\left[1+\left(\frac{E}{E_0}\right)^{S}\right]^{\frac{\Delta\gamma}{S}}\left[1+\left(\frac{E}{E_1}\right)^{S_1}\right]^{\frac{\Delta\gamma_1}{S_1}}$$

Cosmic-ray helium spectrum

PRL 130 171002 (2023)

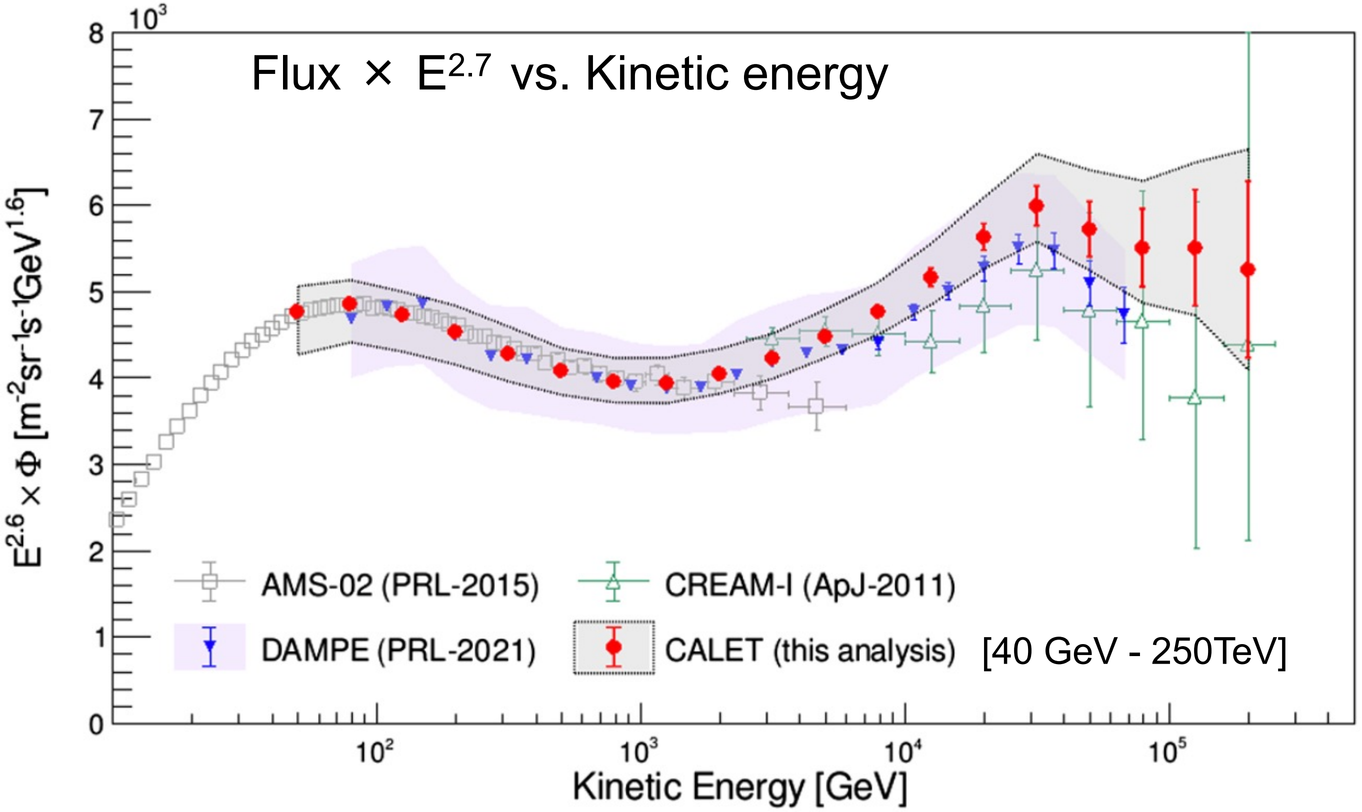

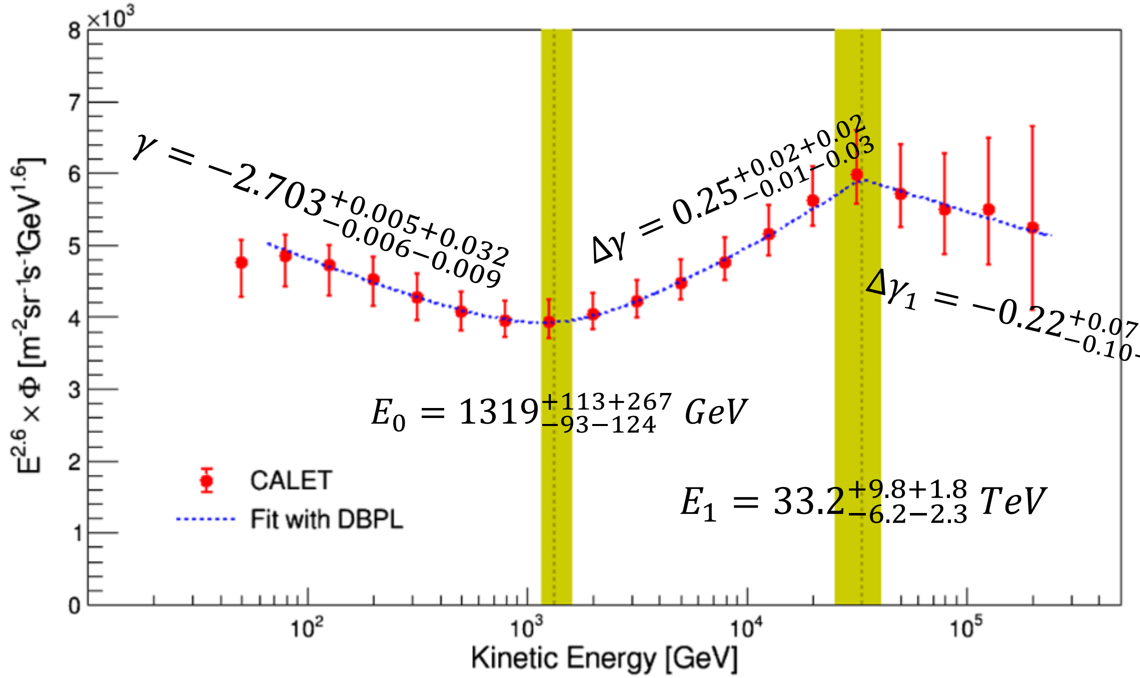

Double Power Law Function: HARDENING SOFTENING

$$\Phi(E) = C\left(\frac{E}{\mathrm{GeV}}\right)^{\gamma}\left[1+\left(\frac{E}{E_0}\right)^{S}\right]^{\frac{\Delta\gamma}{S}}\left[1+\left(\frac{E}{E_1}\right)^{S_1}\right]^{\frac{\Delta\gamma_1}{S_1}}$$

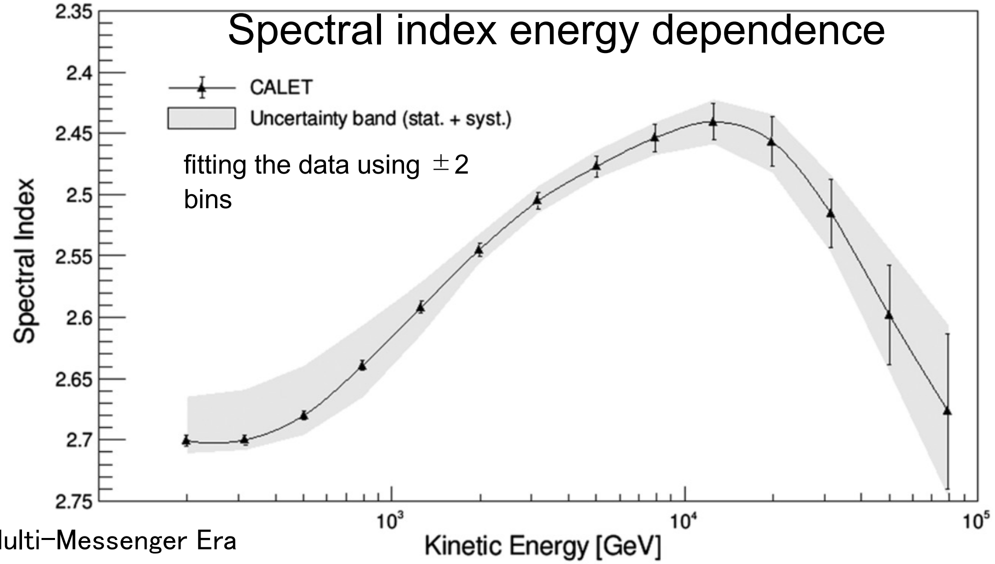

Proton vs. Helium Spectrum

PRL 130 171002 (2023)

Proton & Helium Spectrum vs Energy/nucleon

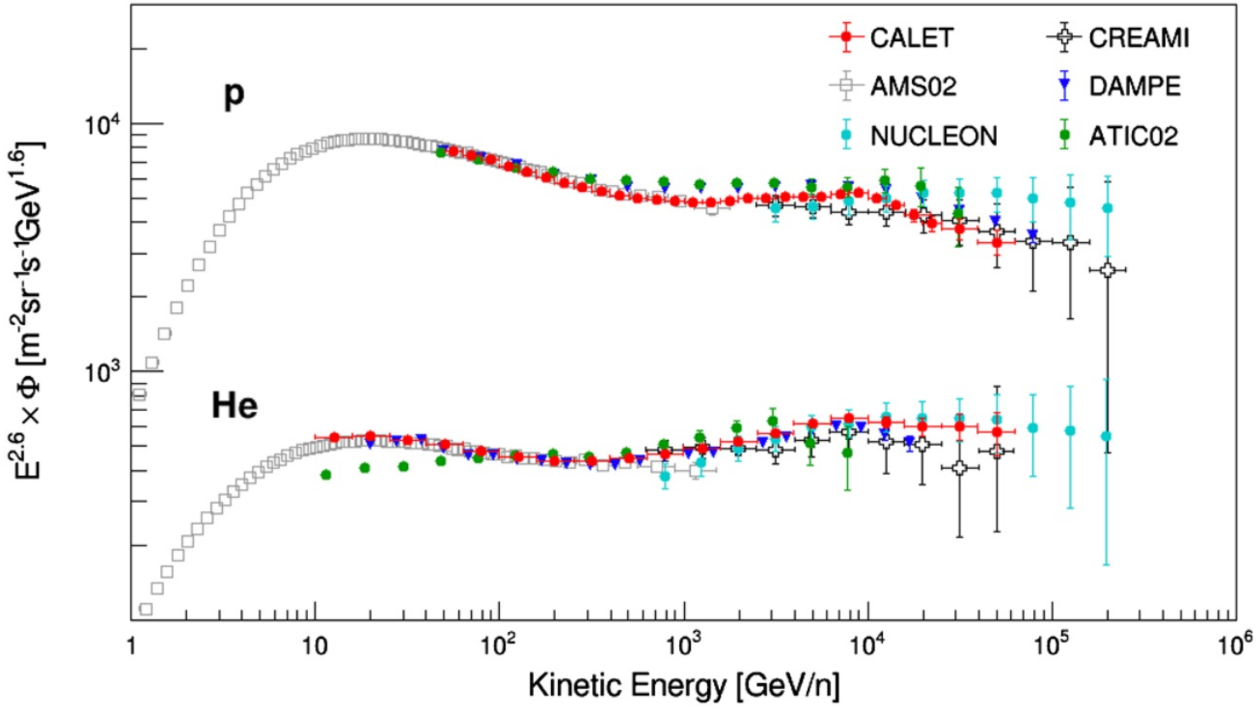

Proton & Helium Spectrum vs Rigidiy

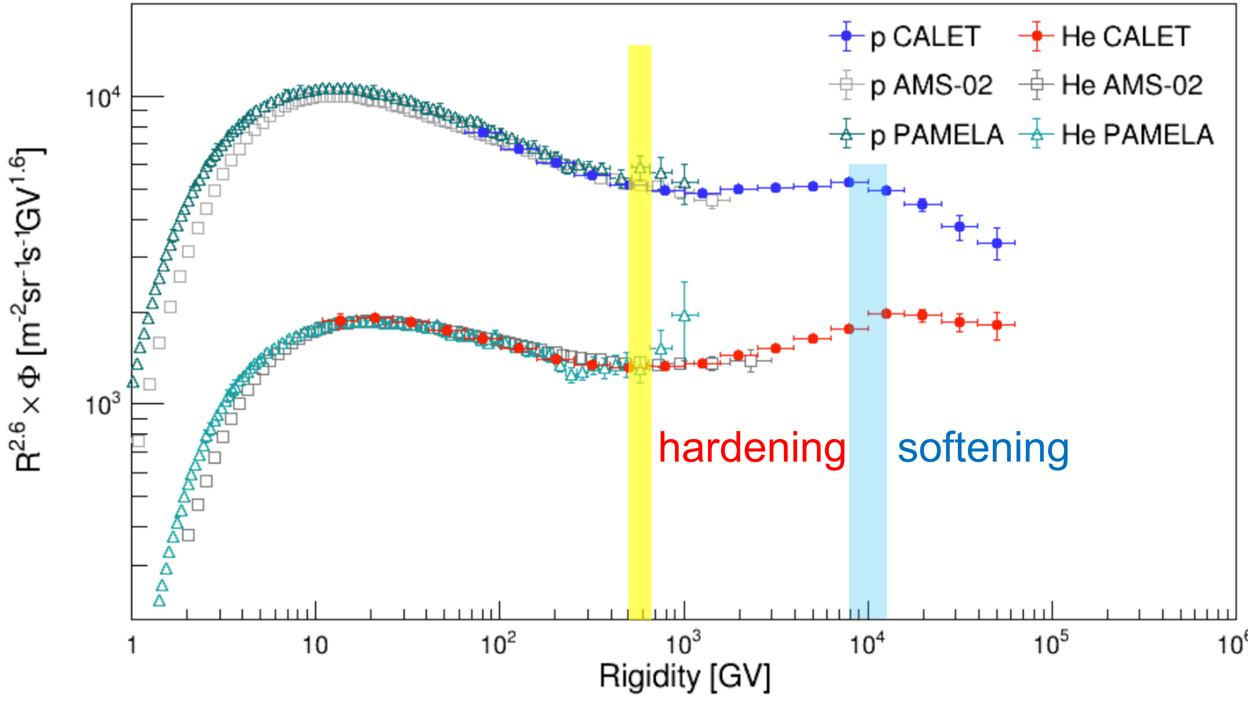

- Both of proton and helium spectrum have a similar structure of hardening and softening around the same region of rigidities.
- The softening of p & He spectrum around 10 TV indicates a possible relation to the energy limit of shock wave acceleration in SNR.

Proton/Helium Ratio

PRL 130 171002 (2023)

Proton/Helium Ratio vs. Energy/nucleon

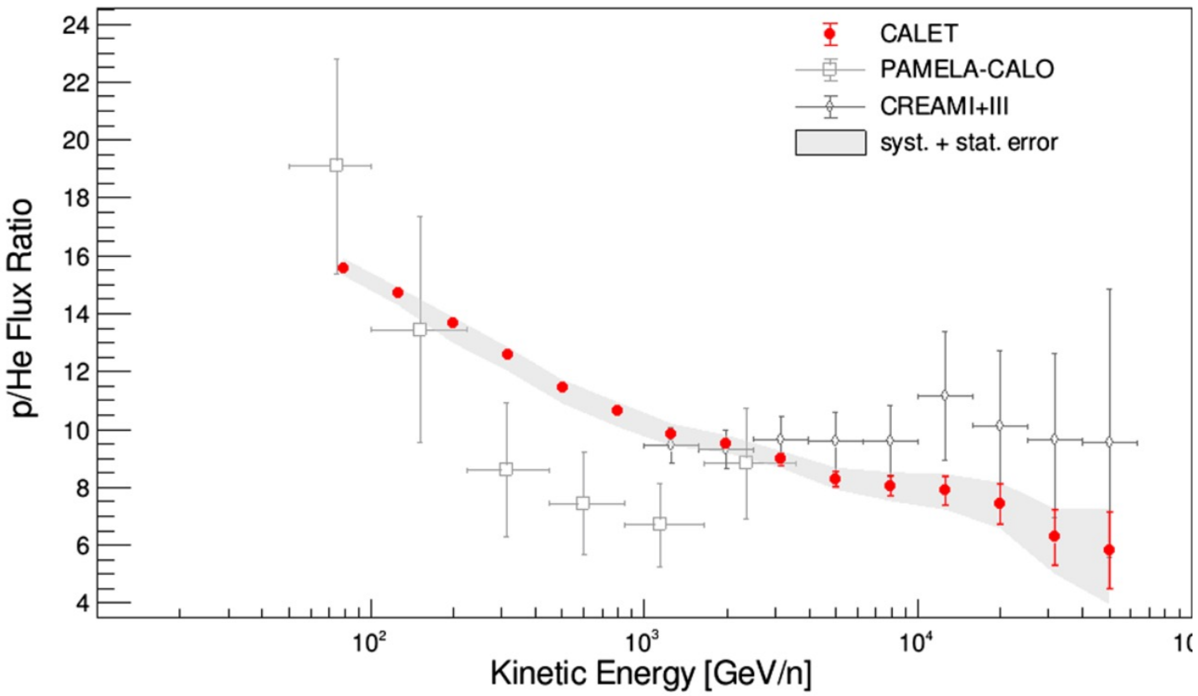

Proton/Helium Ratio vs. Rigidity

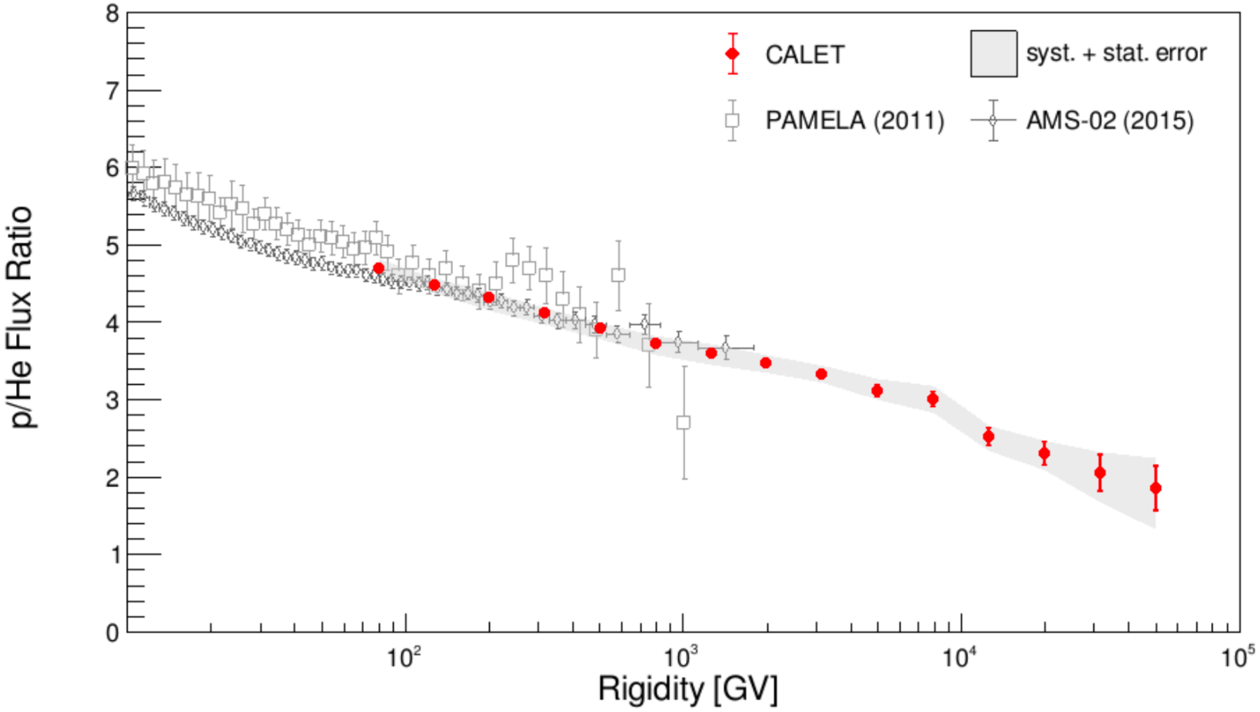

- The spectral index of helium is harder than that of proton (by ~0.1) in the whole rigidity range.
- Possible change of the spectral index of p/He ratio seen above 10 TV will be carefully checked by analyzing higher statistics data in future.

Charge Identification with CHD and IMC

Low Energy

High Energy

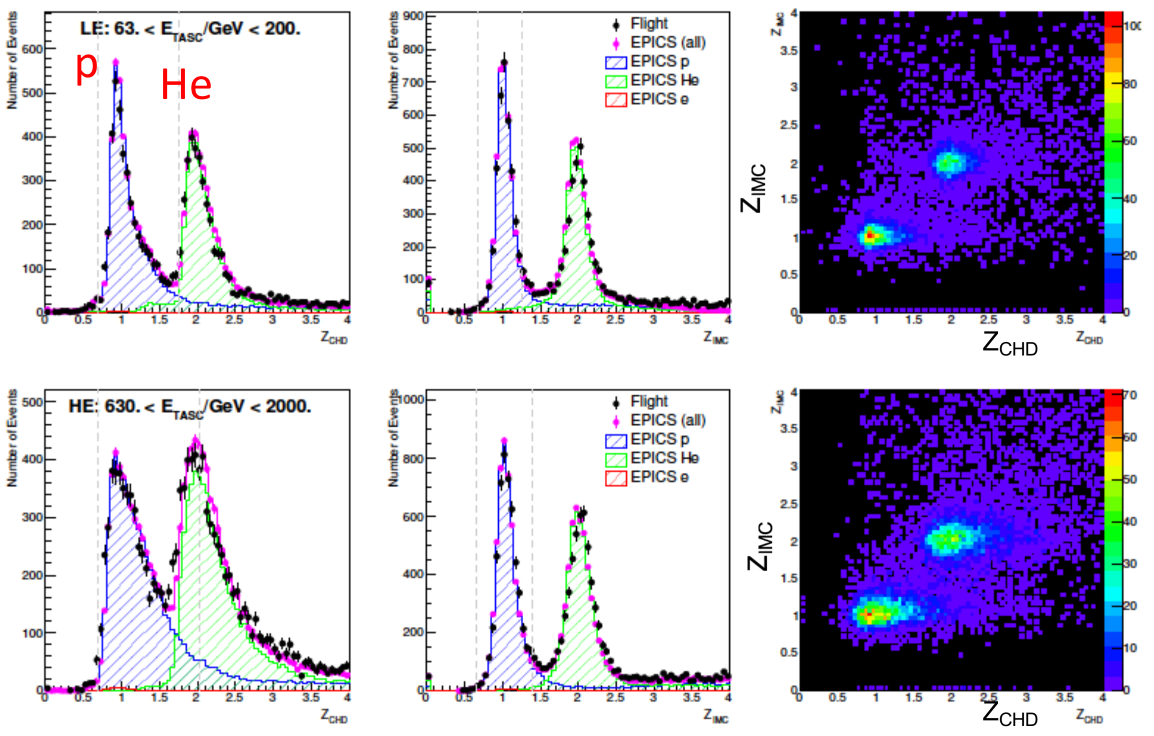

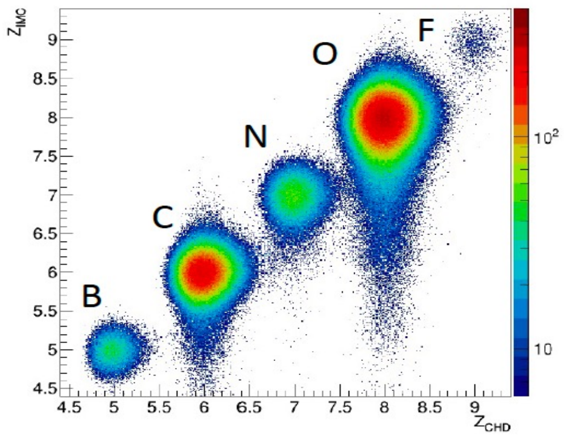

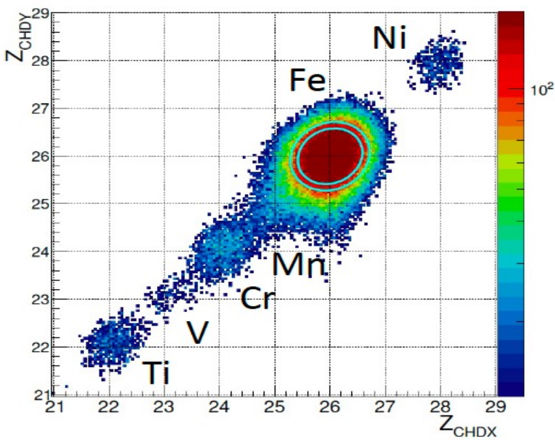

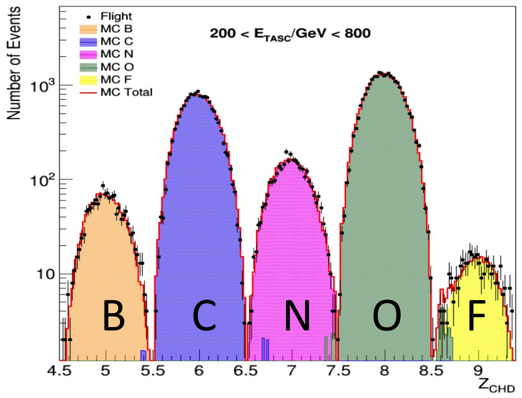

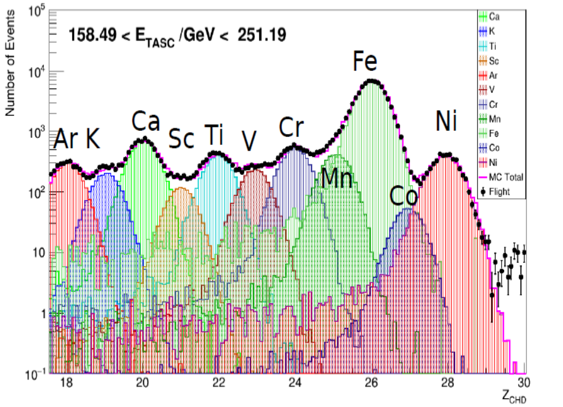

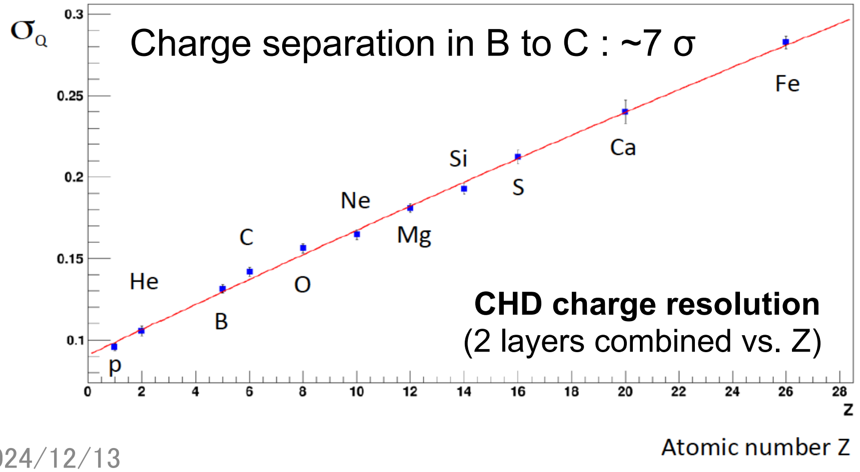

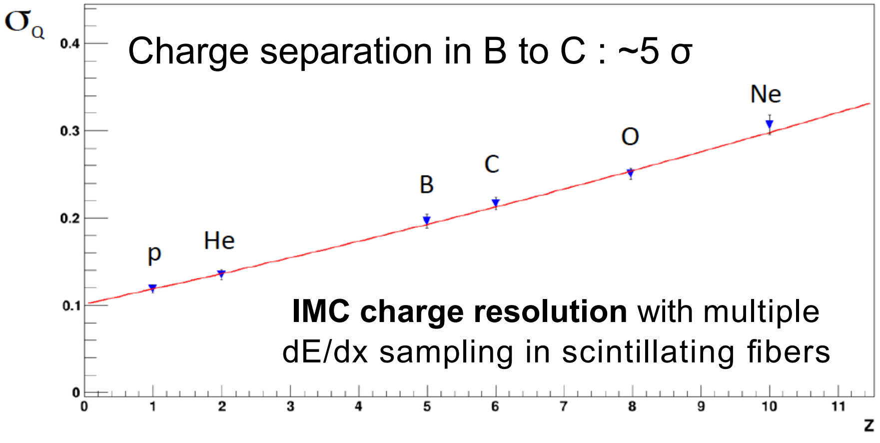

- Single element identification for p, He and light nuclei is achieved by CHD+IMC charge analysis.
- Deviation from Z^2 response is corrected using a core + halo ionization model (Voltz)
- Excellent charge resolution

CHD σ_Z 0.15 e (BCNO) 0.28 (Fe)

IMC σ_Z 0.20 e (BCNO)

Observations of cosmic-ray nuclei from C to Fe

Preliminary spectra of Carbon – Iron

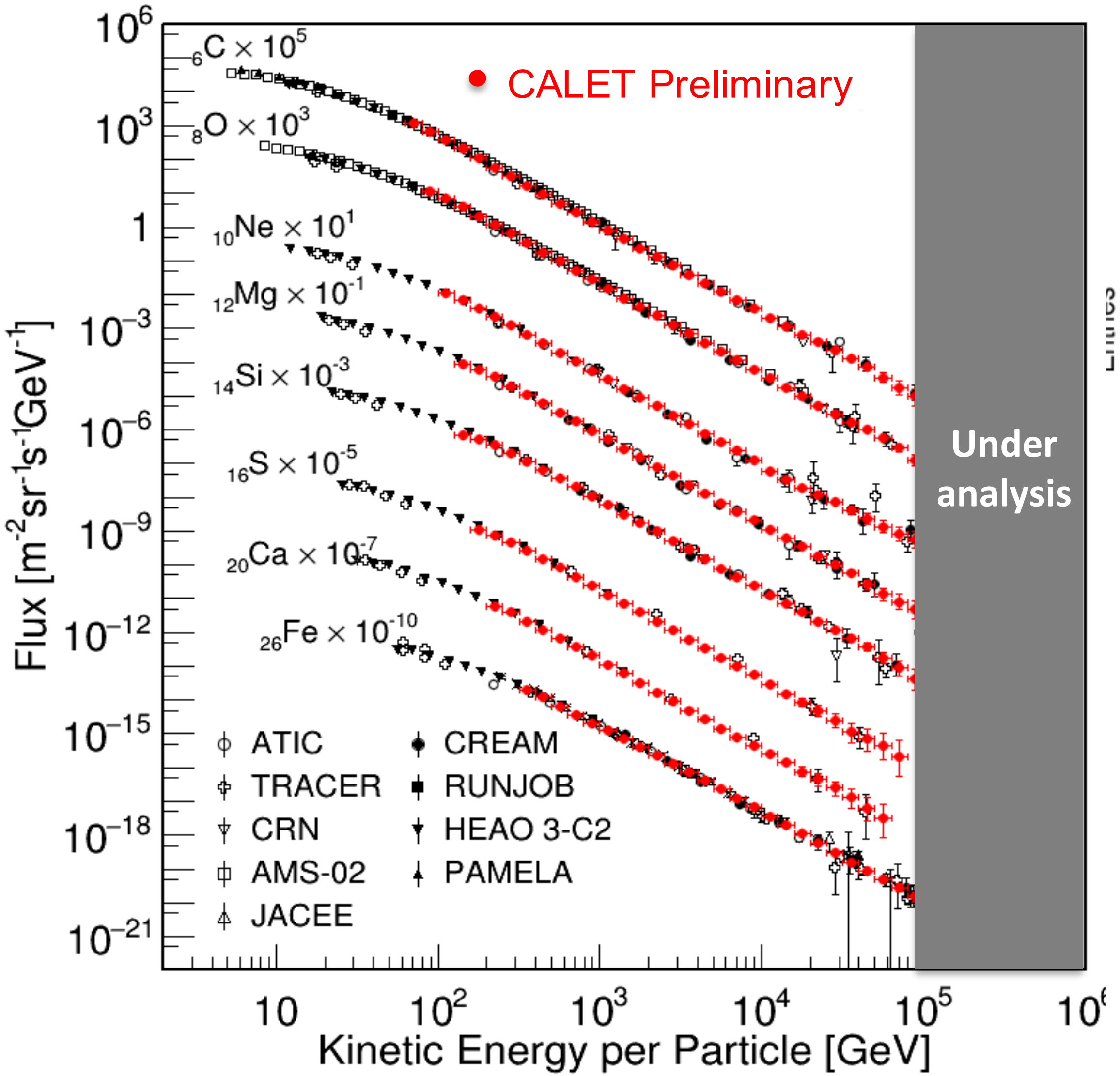

Charge distribution from H to Ni

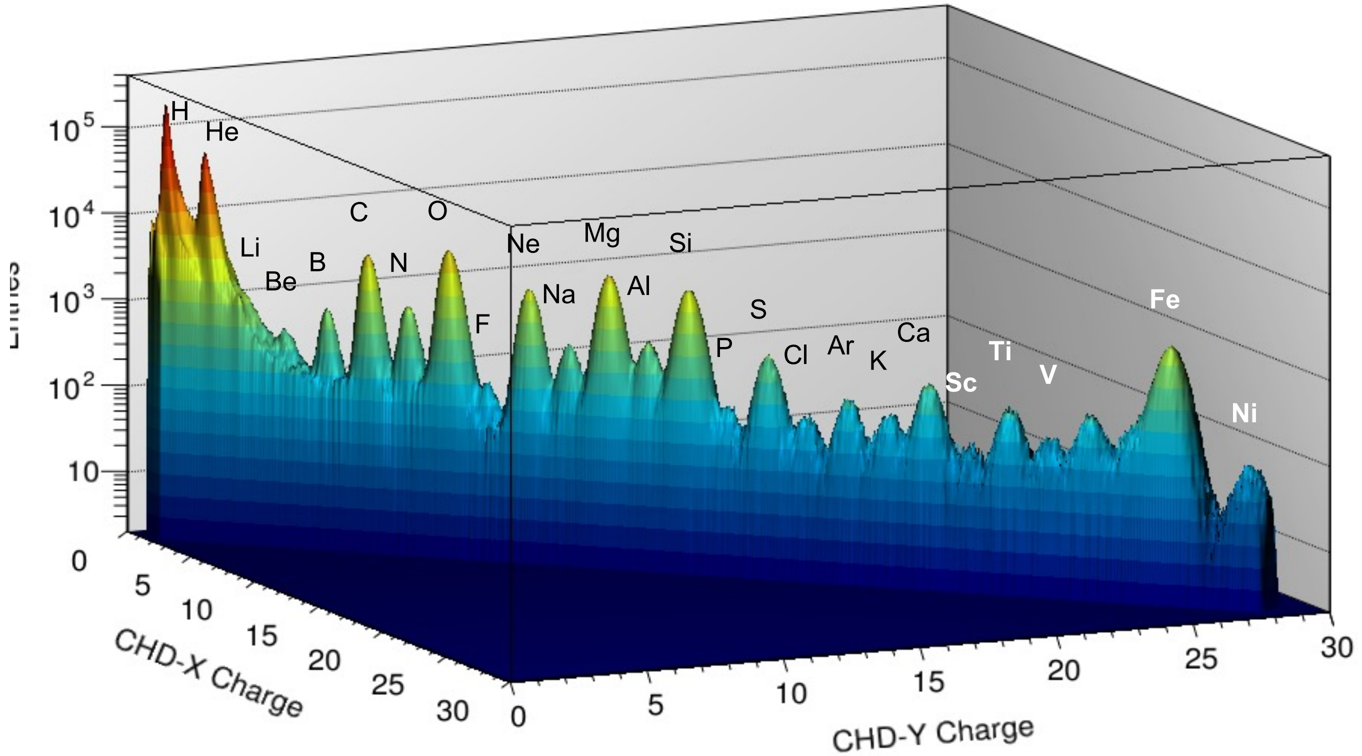

With excellent charge-ID of individual elements CALET is exploring the Table of Elements in the multi-TeV domain

Flux measurement

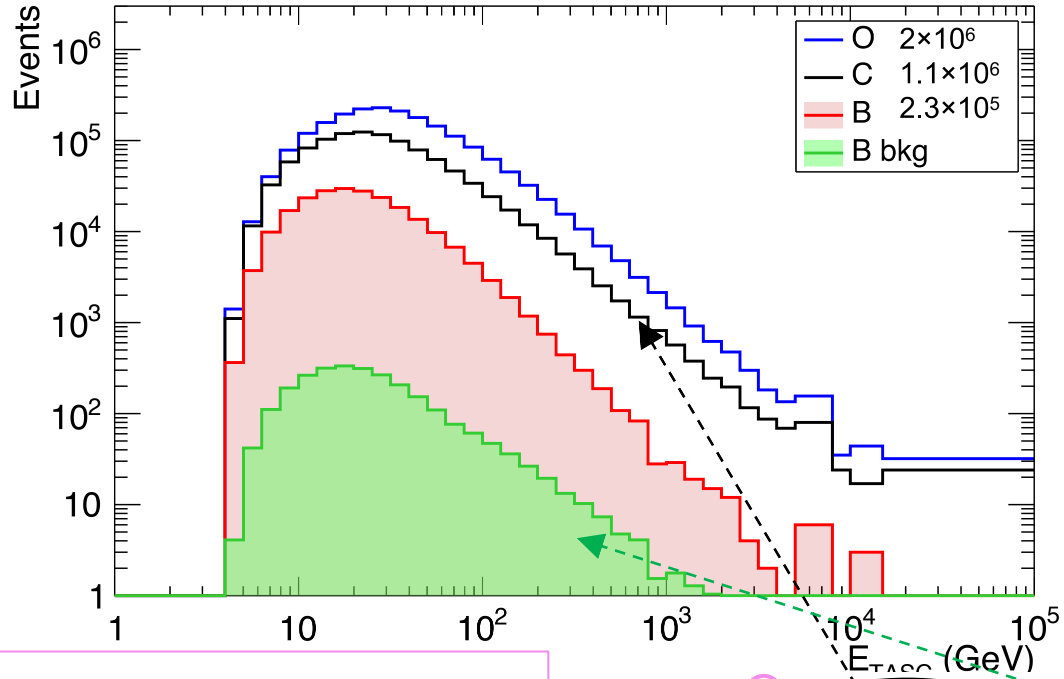

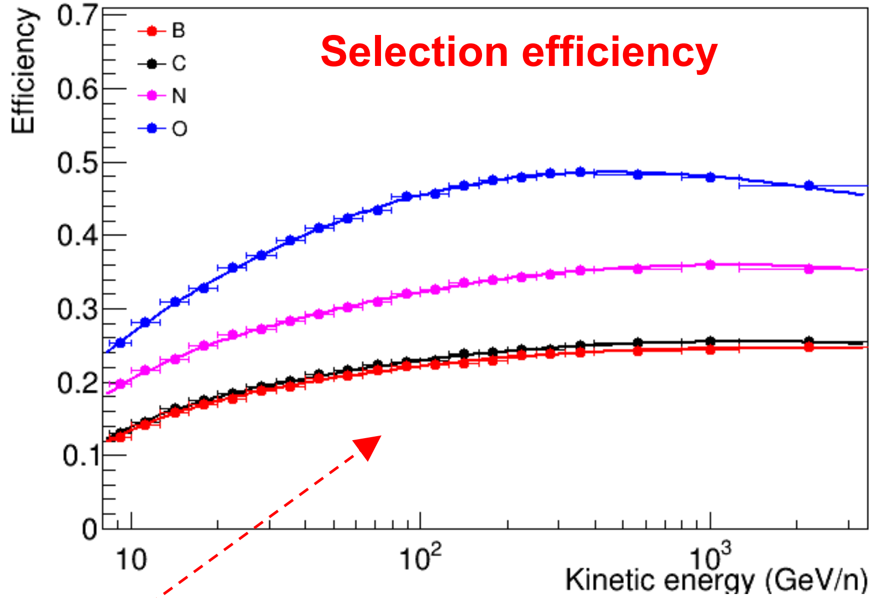

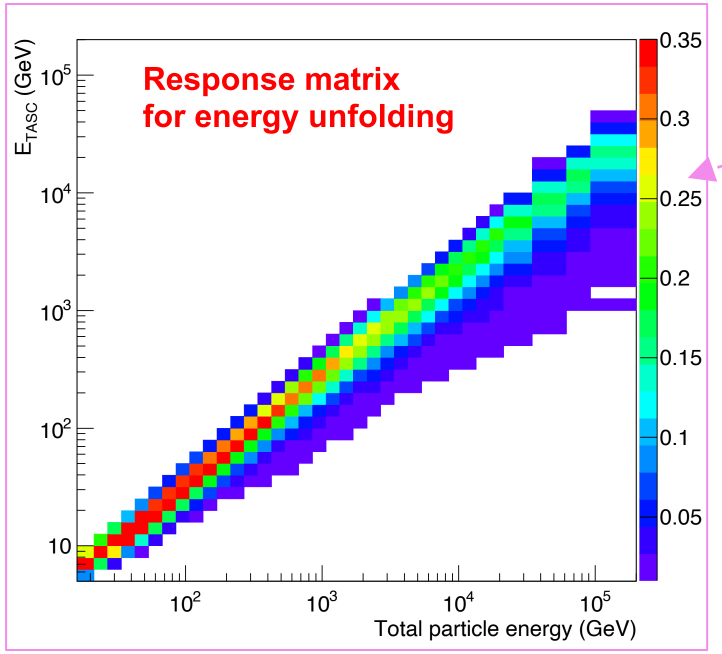

$$N(E) = U\left[N_{obs}(E_{\mathrm{TASC}}) - N_{bg}(E_{\mathrm{TASC}})\right]$$

$$\Phi(E) = \frac{N(E)}{\varepsilon(E)\, S\Omega\, T\, \Delta E}$$

Live time T=86% of observing time (2554 days)

SΩ: 510 cm^2 sr

Bin width ΔE commensurate with rms resolution of TASC , ~30% for nuclei

B C O energy spectra

PRL 125 251102 (2020)
PRL 129 251103 (2022)

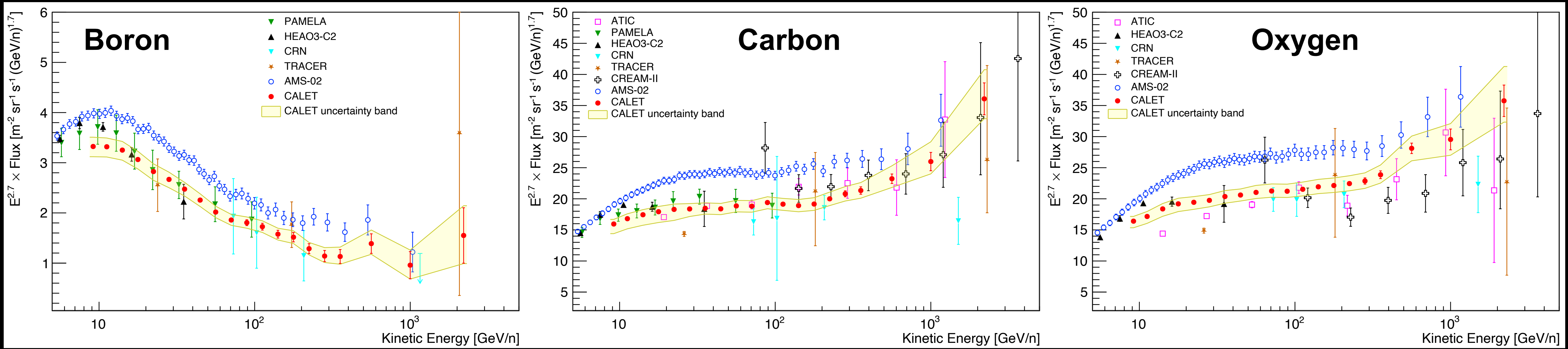

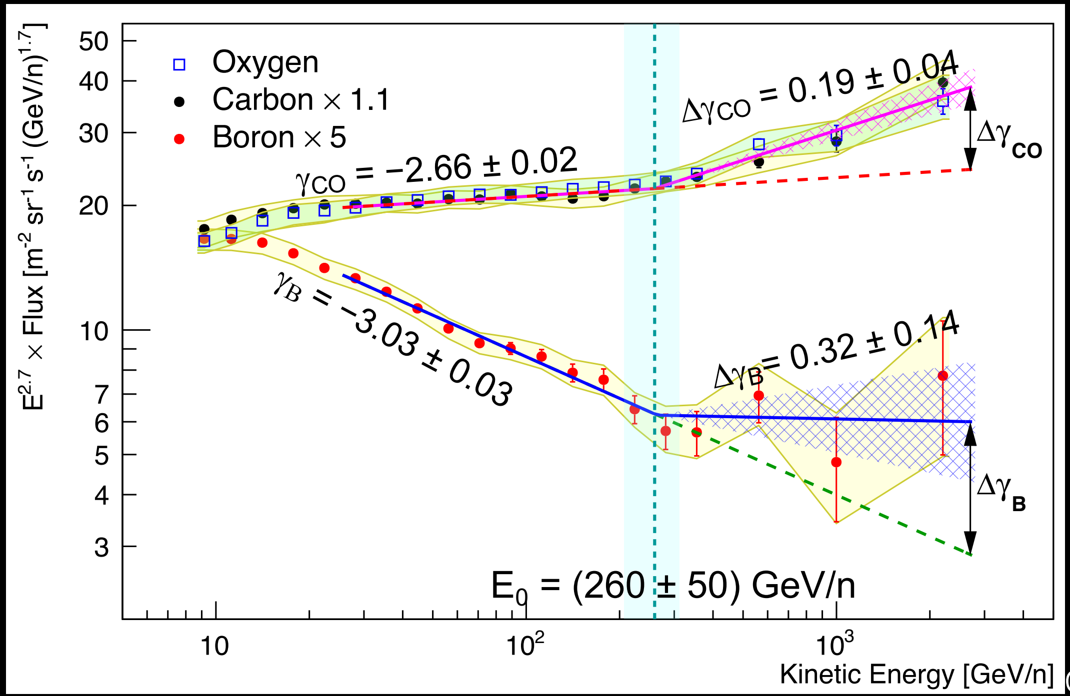

- BCO spectra measured from 8.4 GeV/n to 3.8 TeV/n
- BC fluxes consistent with PAMELA and most previous experiments.
- Similar shape with AMS-02 spectra but lower absolute normalization
- C and O fluxes harden in a similar way above 200 GeV/n
- B spectrum clearly different from C-O as expected for primary and secondary CR
- Fit results seem to indicate, albeit with low statistical significance, that the flux hardens more for B than for C and O above 200 GeV/*n*.

Survival probabilities

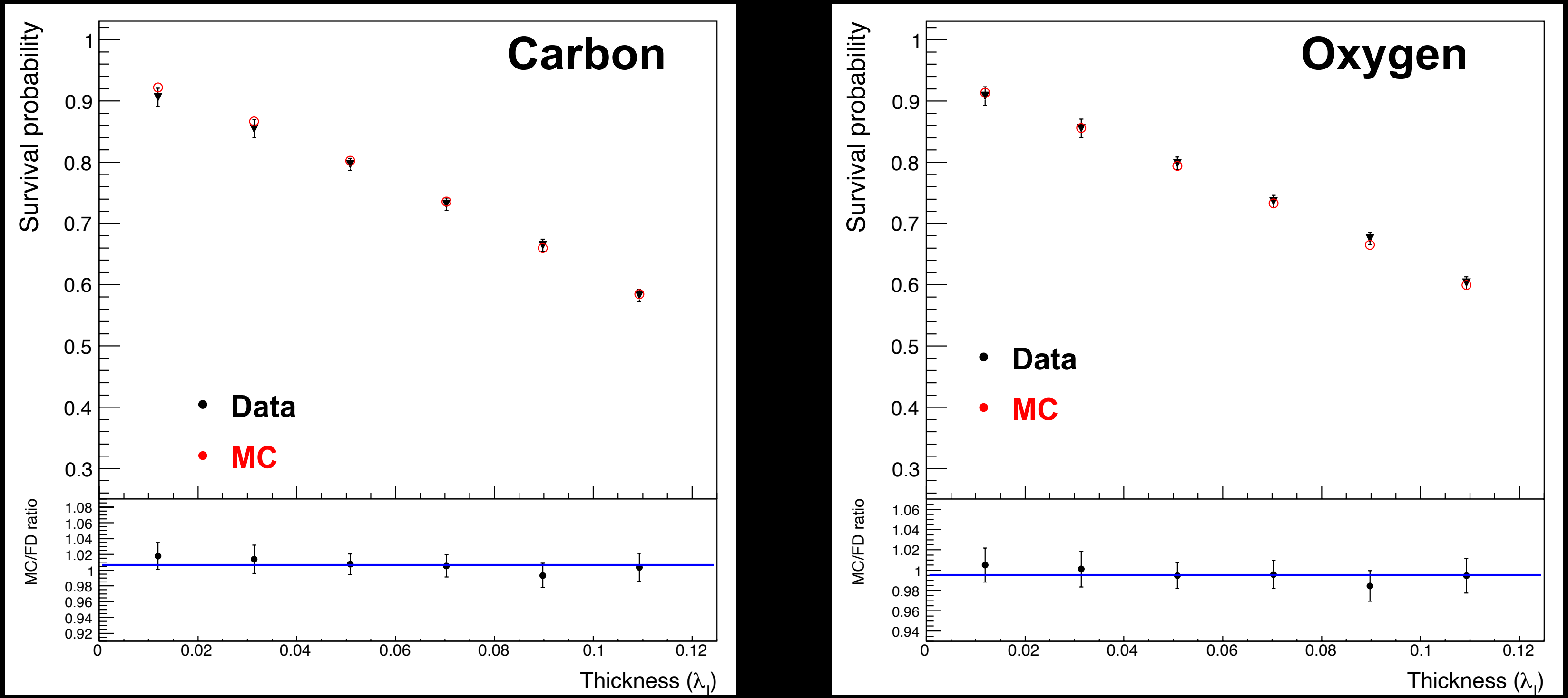

- We measured the survival probabilities of C and O nuclei at different depths in IMC to check that hadronic interactions in the detector are well simulated.

- In flight data, the survival probabilities are calculated as the ratio of the number of events selected as C (O) in the first six pairs of SciFi layers in IMC to the ones selected with CHD only.
  In MC (EPICS) data, the true information on the point where the first hadronic interaction occurs in the detector is used.

- Very good agreement between data and simulation (within <1%).

Monte Carlo models

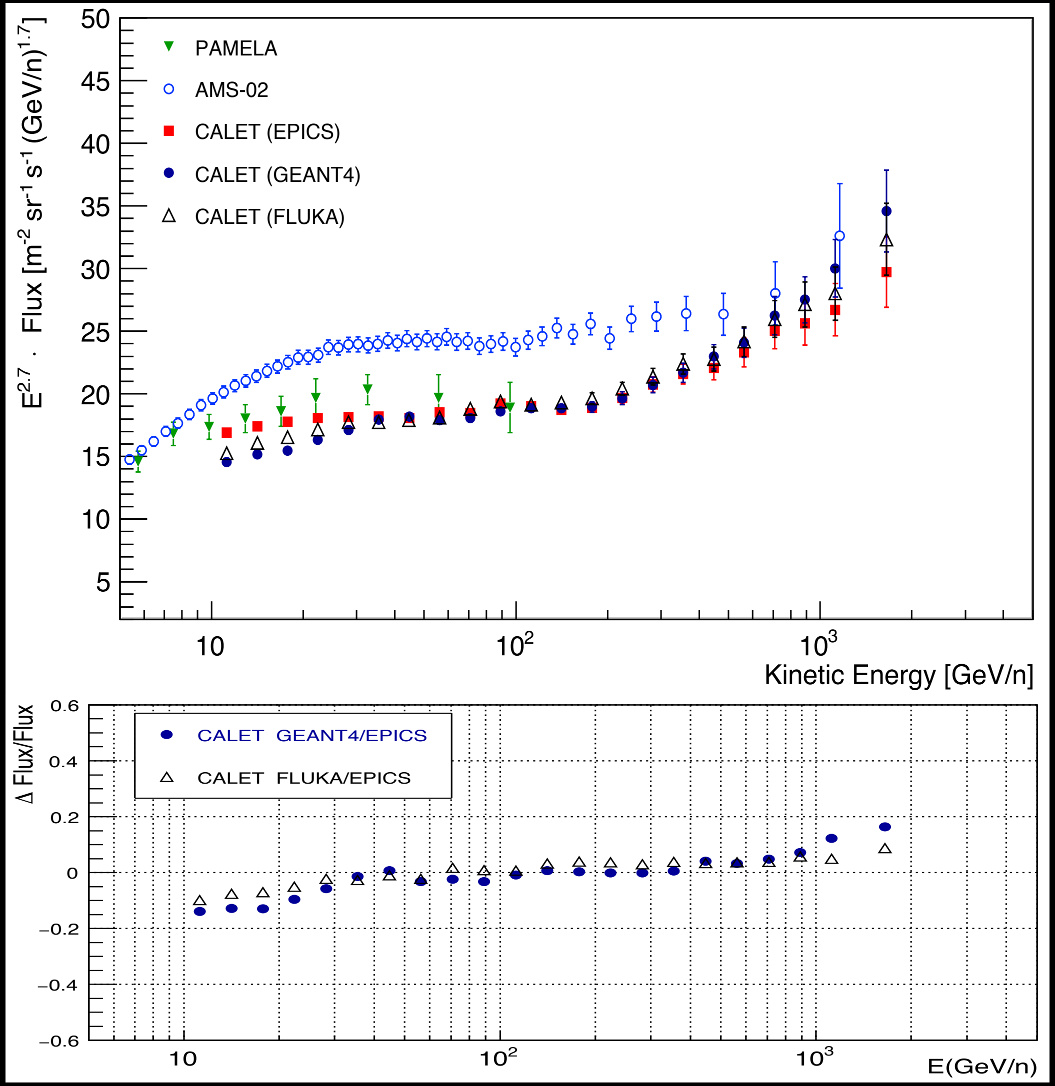

MC simulations, reproducing detector configuration, physics processes, and detector signals, were developed based on three simulation packages

- EPICS 9.21 w/ DPMJET-III
- Fluka 2011 2c.6 w/ DPMJET-III
- GEANT4 10.5 w/ FTFP_BERT

MC simulations were tuned using beam test and flight data.

They are used to estimate selection efficiencies and response matrix.

Comparison of energy responses from different MC at high energy where no beam calibration is available.

The resultant fluxes from the analyses with different MC's show consistent normalization and spectral shapes.

B C O flux ratios

PRL 125 251102 (2020)
PRL 129 251103 (2022)

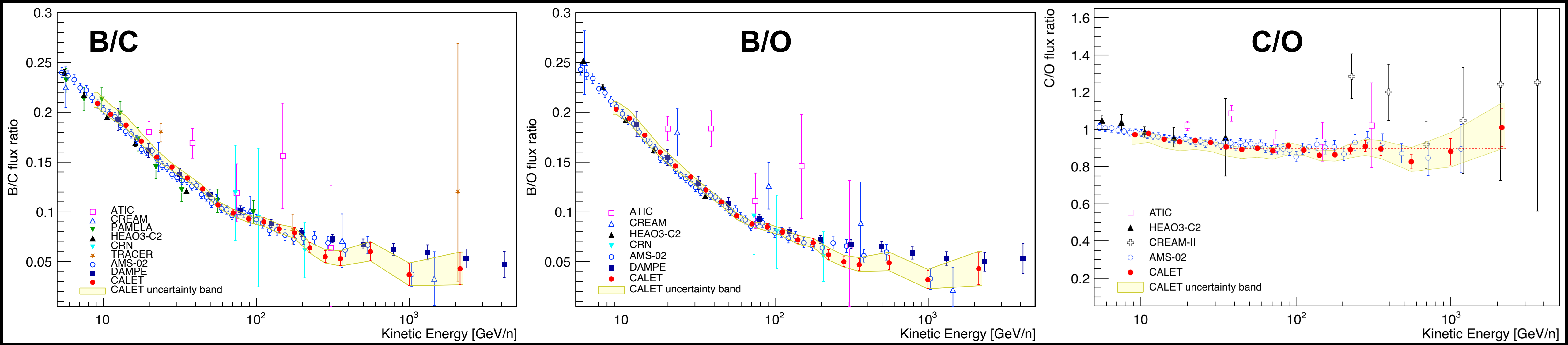

- Flux ratios of B/C and B/O are in agreement with AMS02 and lower than DAMPE result above 300 GeV/n, although consistent within the error bars.
- C/O flux ratio as a function of energy is in good agreement with AMS-02.
- At E > 30 GeV/n the C/O ratio is well fitted to a constant value 0.90 ± 0.03 → C and O fluxes have the same energy dependence.
- At E < 30 GeV/n C/O ratio is slightly softer → secondary C from O and heavier nuclei spallation

Spectral fit of B/C and B/O

PRL 125 251102 (2020)
PRL 129 251103 (2022)
ICRC2023 PoS 058

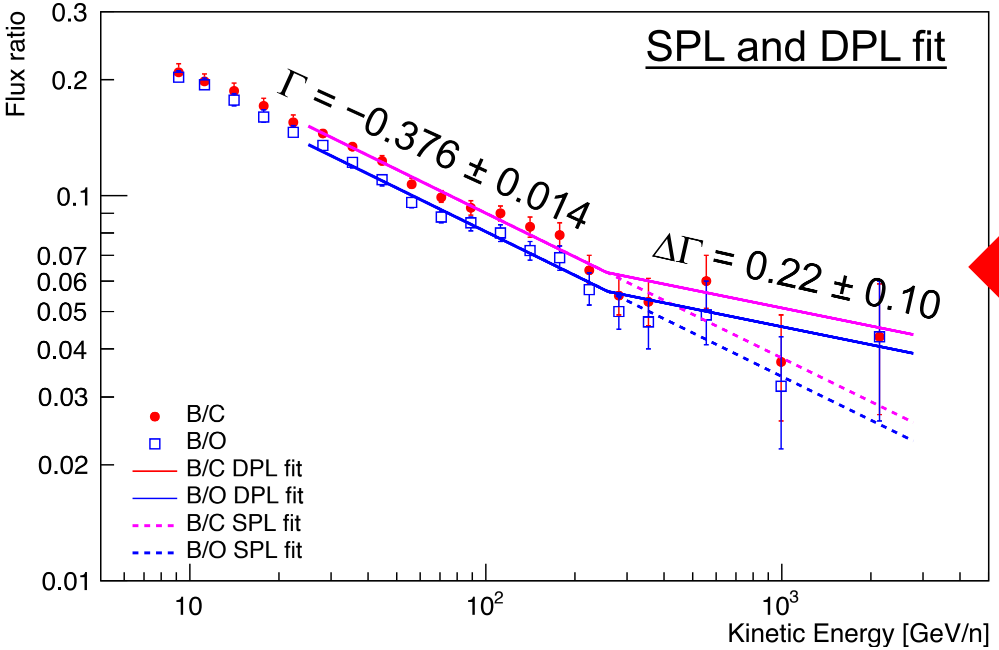

Simultaneous fit to B/C and B/O (E>25 GeV/n) with same parameters except normalization.
DPL fit suggests, though with currently limited statistical significance, a flattening of the B/C ratio at high energy, consistent with AMS-02 and DAMPE.
This supports the hypothesis that secondary B exhibits a stronger hardening than primary C and O.

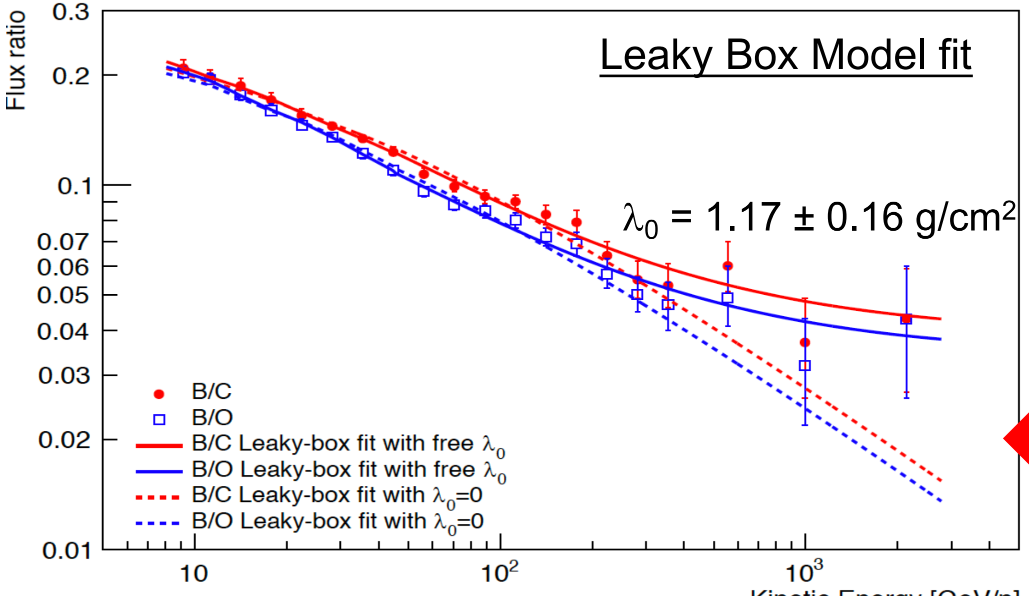

$$\frac{\Phi_B(E)}{\Phi_C(E)} = \frac{\lambda(E)\lambda_B}{\lambda(E)+\lambda_B}\left[\frac{1}{\lambda_{C\to B}} + \frac{\Phi_O(E)}{\Phi_C(E)}\frac{1}{\lambda_{O\to B}}\right]$$

$$\frac{\Phi_B(E)}{\Phi_O(E)} = \frac{\lambda(E)\lambda_B}{\lambda(E)+\lambda_B}\left[\frac{1}{\lambda_{O\to B}} + \frac{\Phi_C(E)}{\Phi_O(E)}\frac{1}{\lambda_{C\to B}}\right]$$

The escape pathlength can be parametrized as $\lambda(E) = kE^{-\delta} + \lambda_0$

Significance of $\lambda_0 \neq 0$ > 5σ → Residual path length could explain the flattening of B/C, B/O ratios at high energies.

Iron and nickel spectra

PRL 126 241101 (2022)
PRL 128 131103 (2023)
ICRC2023 PoS 061

Flux × $E^{2.6}$ vs kinetic energy per nucleon

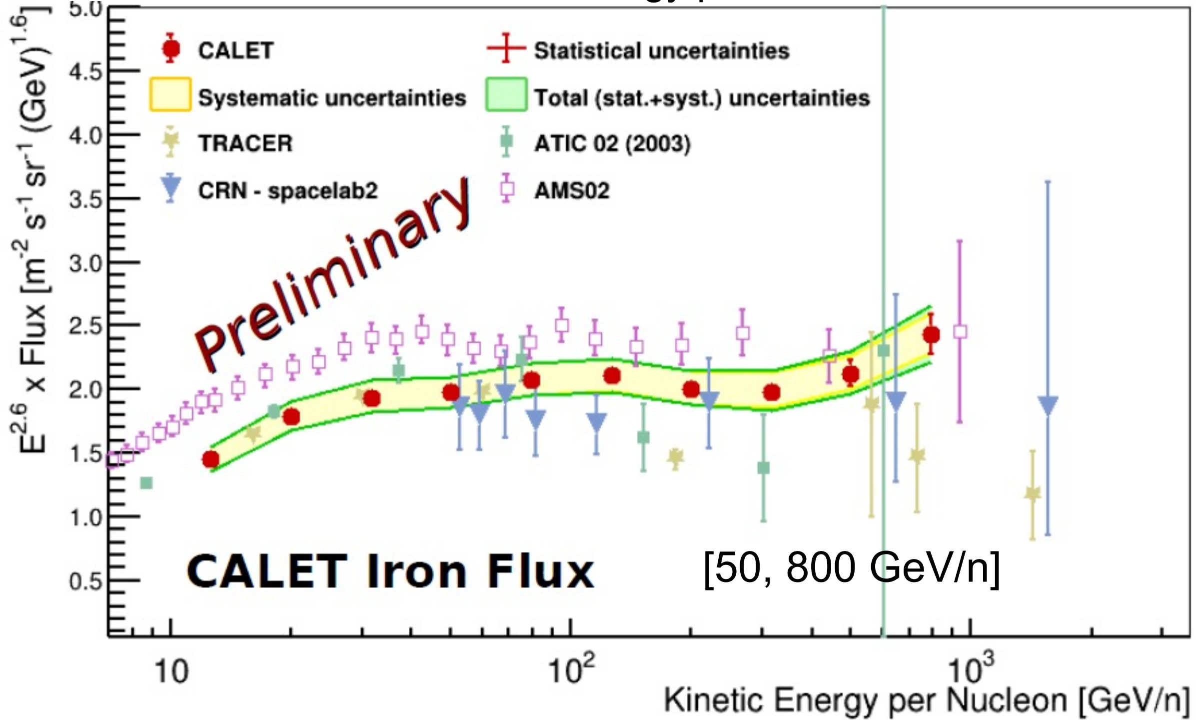

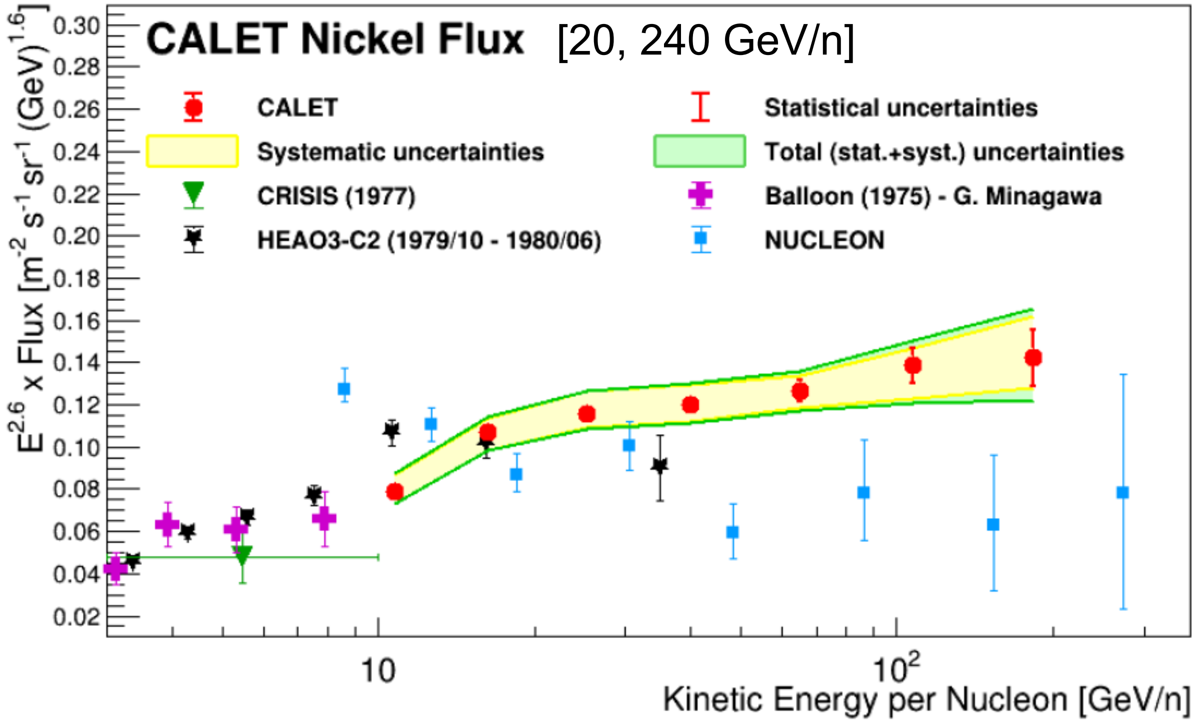

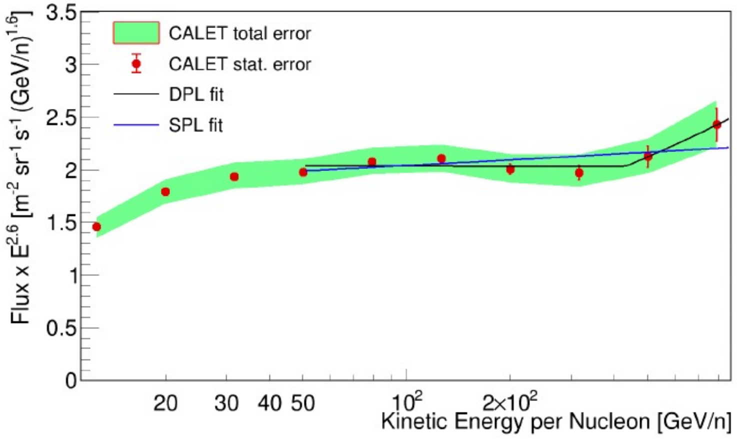

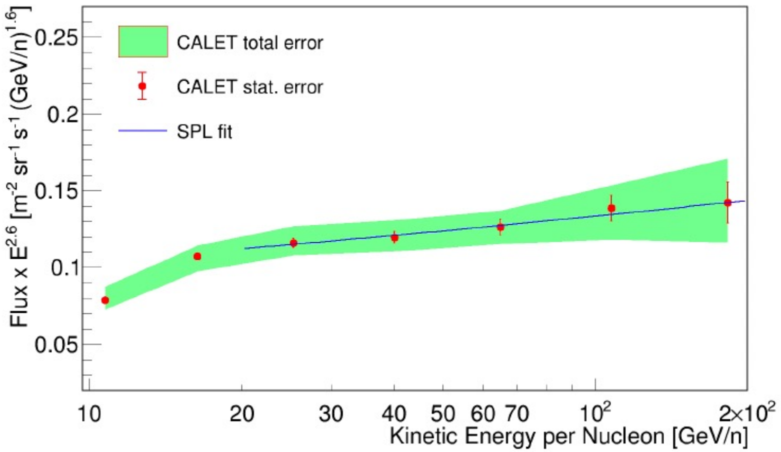

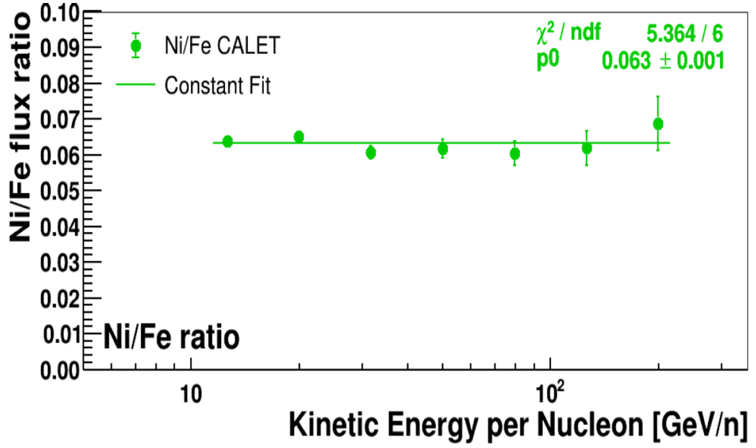

Flux ratios between primary elements

ICRC2023 PoS 058

C/He and O/He ratio

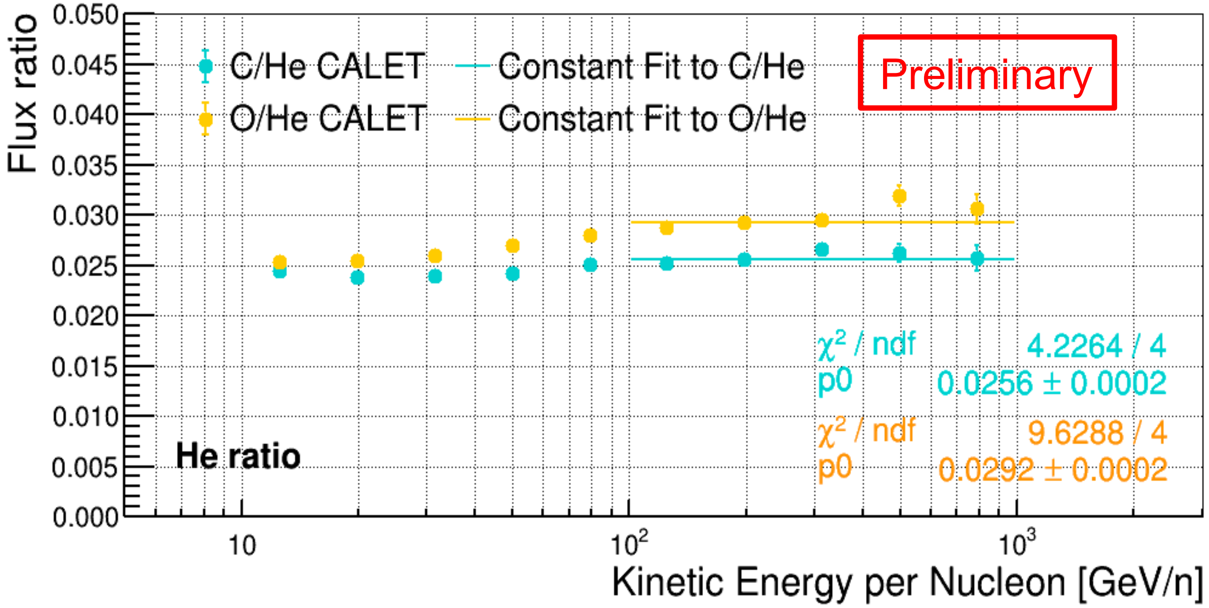

Fe/C Fe/O Fe/He ratios

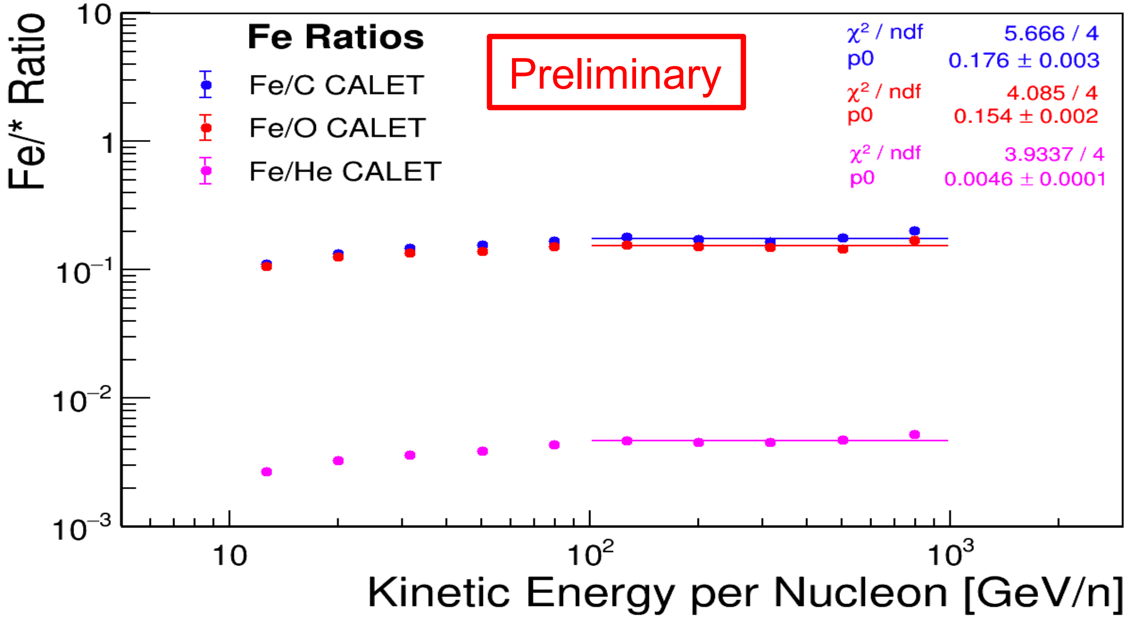

The flux ratio between light nuclei (He, C, O) is constant above 100 GeV/n
Fe/O, Fe/C and Fe/He ratios are compatible with a constant above 100 GeV/n within errors → similar propagation

Ultra-heavy cosmic-ray nuclei (26 < Z ≤ 44)

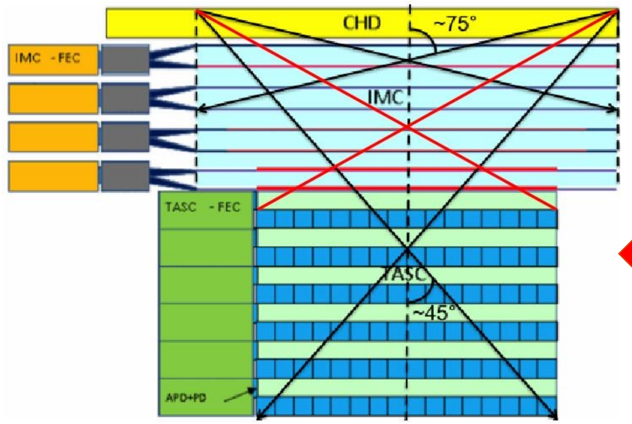

- Special UH trigger with **GF ~ 4400 cm^2**
- ~260 million events collected
- Energy measurement based on rigidity cutoff. TASC used for a sub-sample of events (65 million)

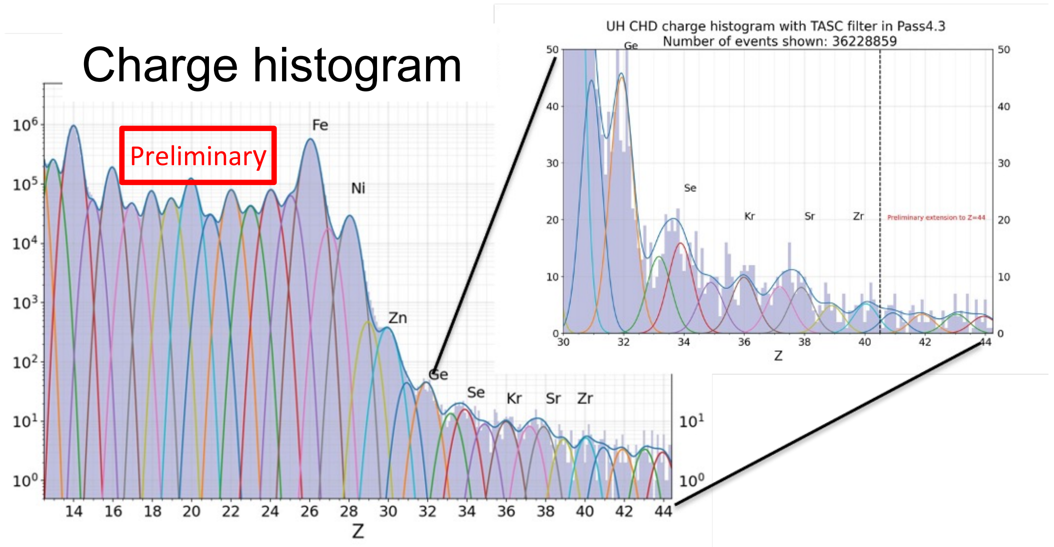

Measurement of the relative abundances of the elements above Fe up to $_{44}$Ru (Fe =1)

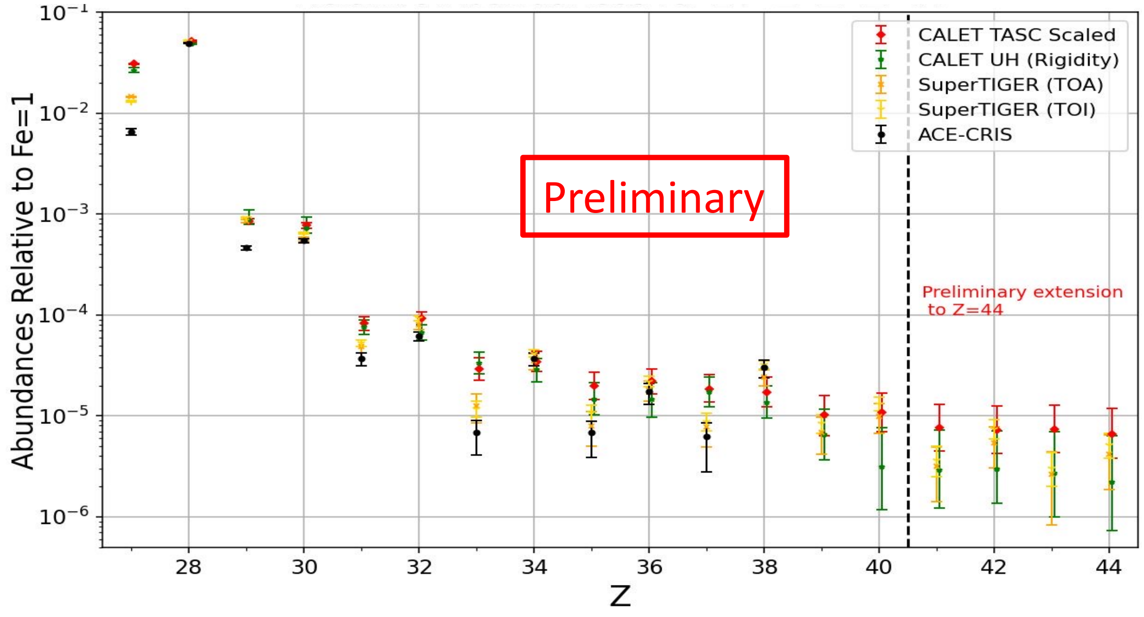

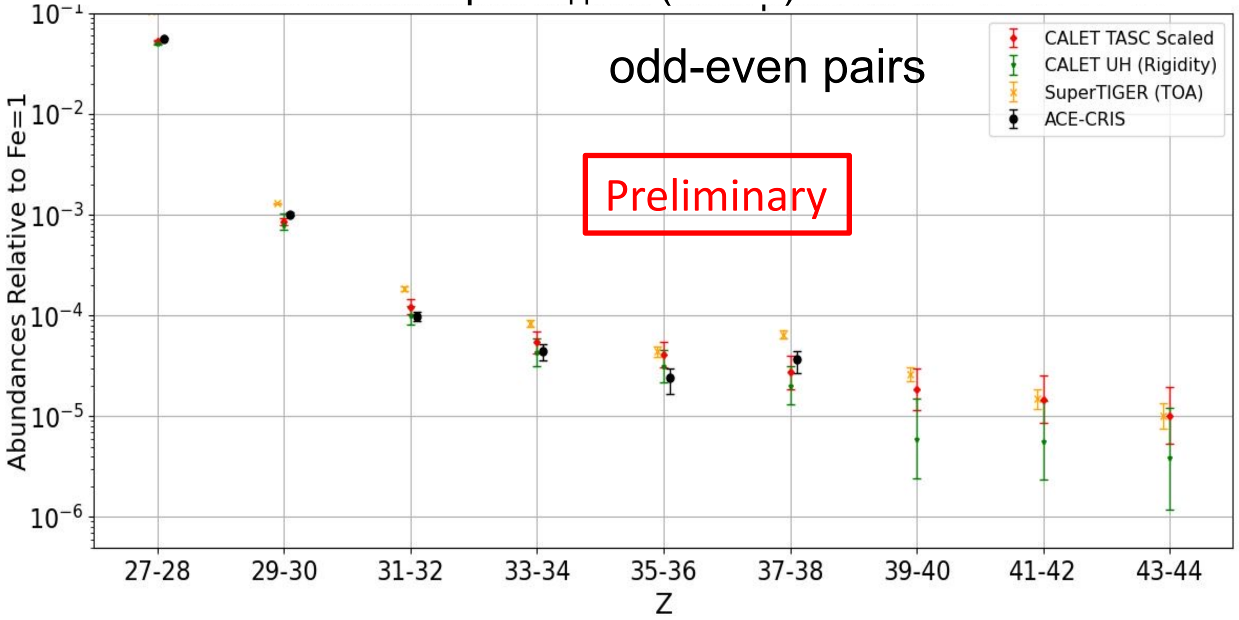

CALET: Summary and Future Prospects

- CALET was launched on Aug. 19th, 2015. The observation campaign started on Oct. 13th, 2015.
  Excellent performance and remarkable stability of the instrument have been confirmed.

- As of Aug. 31, 2024, total observation time is 3200 days with live time fraction close to 86%.
  Nearly 4.78 billion events collected with low energy trigger (> 1 GeV) and 2.15 billion events with high energy trigger

- Accurate calibrations have been performed in the energy measurements established in 1 GeV-1PeV.

- Analysis of cosmic-ray events continues, extending to higher energies and charges
  - All electron spectrum in the range 10.6 GeV – 7.5 TeV.
  - Proton spectrum in the range 50 GeV – 60 TeV
  - Helium spectrum in the range 40 GeV – 250 TeV
  - BCO spectra in the range 8.4 GeV/n – 3.8 TeV/n
  - B/C flux ratio up to 3.8 TeV/n
  - Iron spectrum in the range 50 GeV/n – 2 TeV/n
  - Nickel spectrum in the range 8.8 GeV/n – 240 GeV/n
  - Abundances of heavy and ultra-heavy nuclei ($13 \leq Z \leq 44$)

- CALET has successfully completed 9 years of observations and has been **approved by JAXA/NASA/ASI for extended operations until 2030!**

Backup slides

Selection for B,C,O candidate events

- High-Energy shower trigger: coincidence of signals (>50 MIP) in last IMC layers and signal (>100 MIP) in top TASC layer.
- Rejection of events entering from lateral sides by analyzing longitudinal and lateral shower profiles
- KF tracking. Track quality cuts.
- Acceptance (events crossing top CHD, TASC top and bottom excluding 2 cm from the edges)
- FOV cut: events (8%) pointing to ISS structures are discarded based on FOV maps

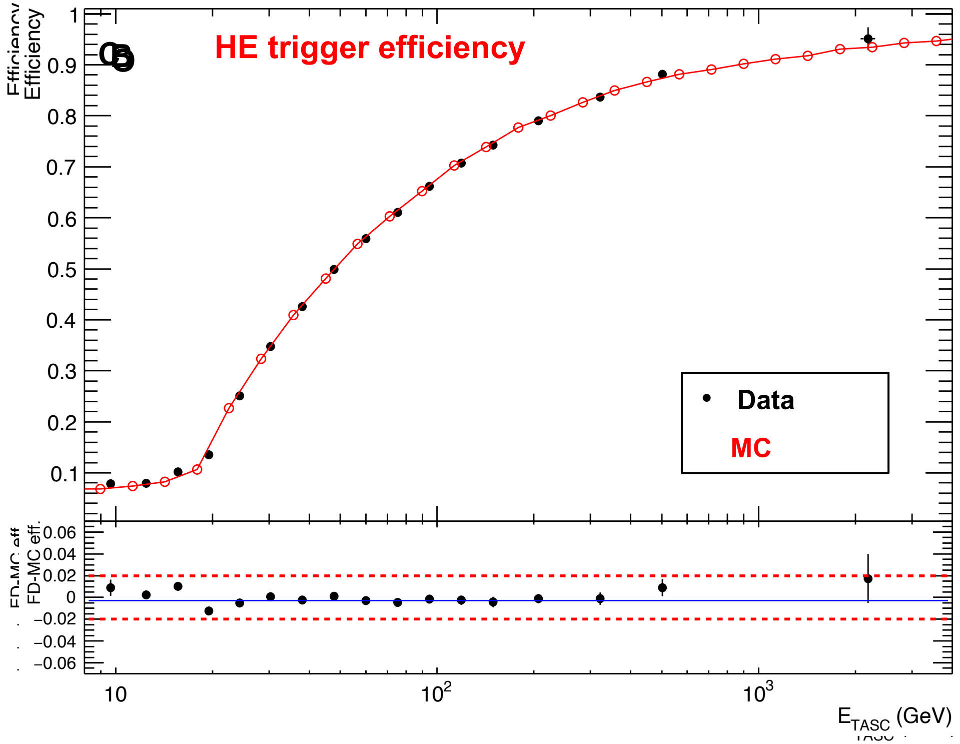

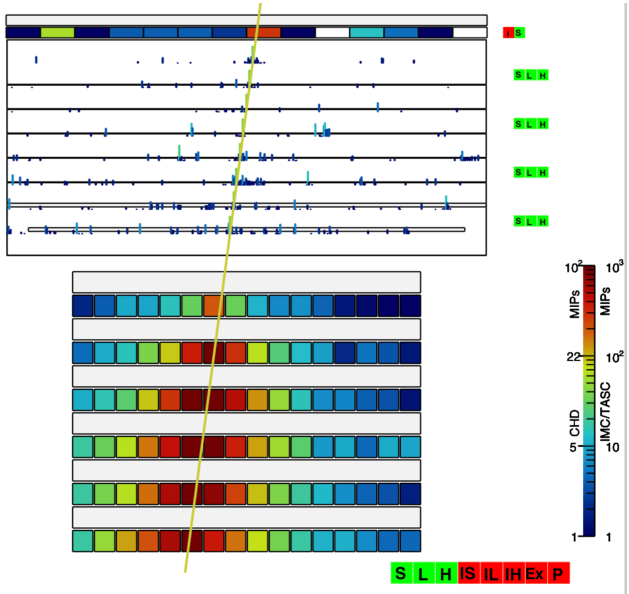

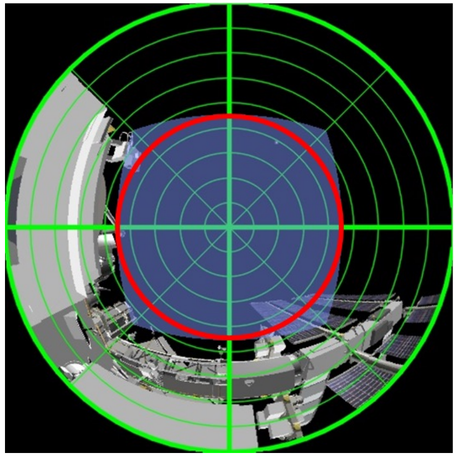

Systematic Uncertainties

We check the stability of the spectrum by varying the analysis cuts and w/ different MC simulations for efficiencies and unfolding.

Main sources of systematics uncertainties:

- **Normalization:**
  - Live time
  - Long-term stability
  - Energy scale
- **Energy dependent:**
  - Tracking
  - Charge ID
  - Trigger
  - Unfolding
  - MC model (EPICS, GEANT4)
  - Background subtraction
  - B isotopic composition (ref. $^{11}B:^{10}B = 0.7:0.3$)

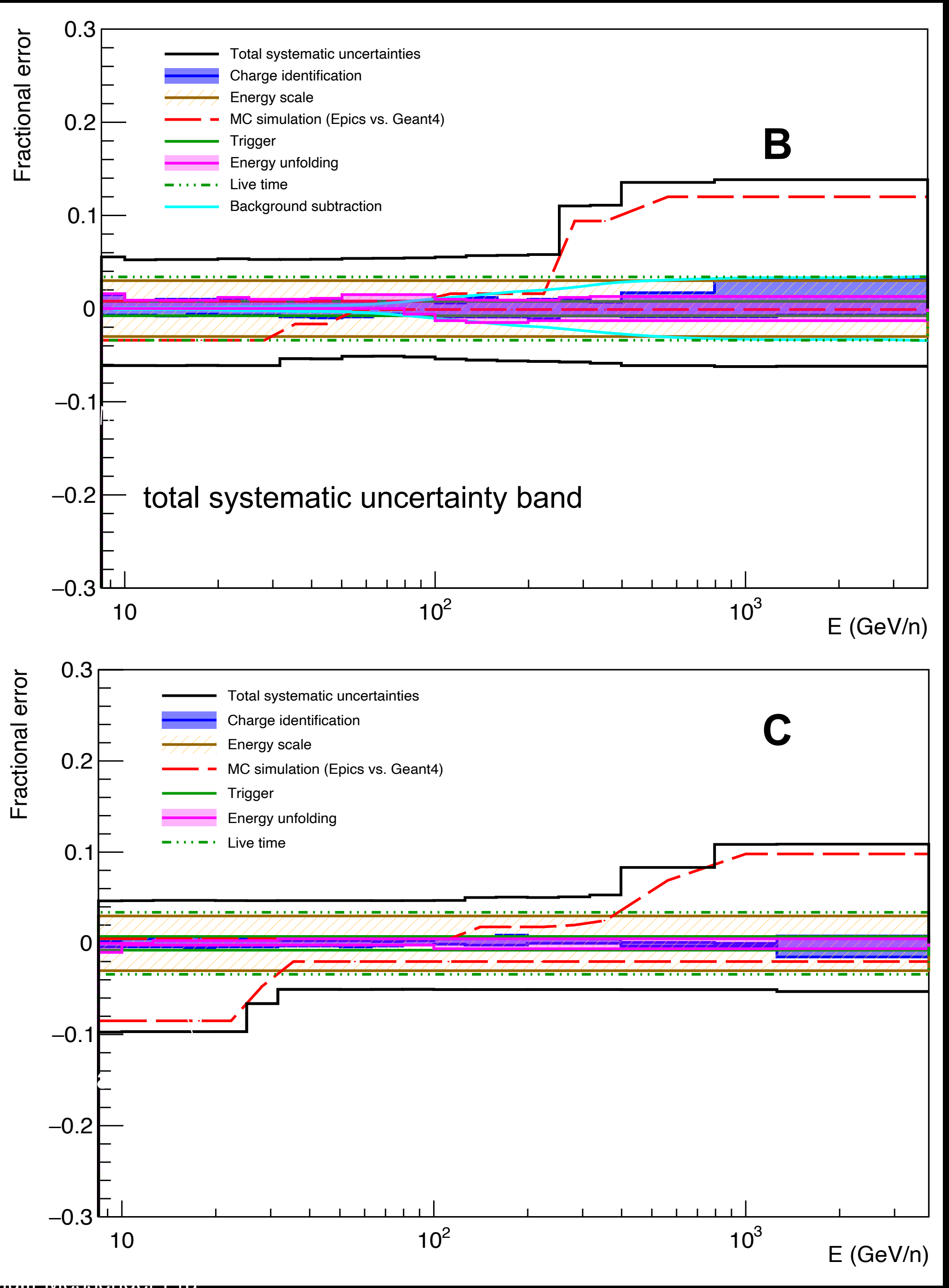

High vs. low-energy triggers

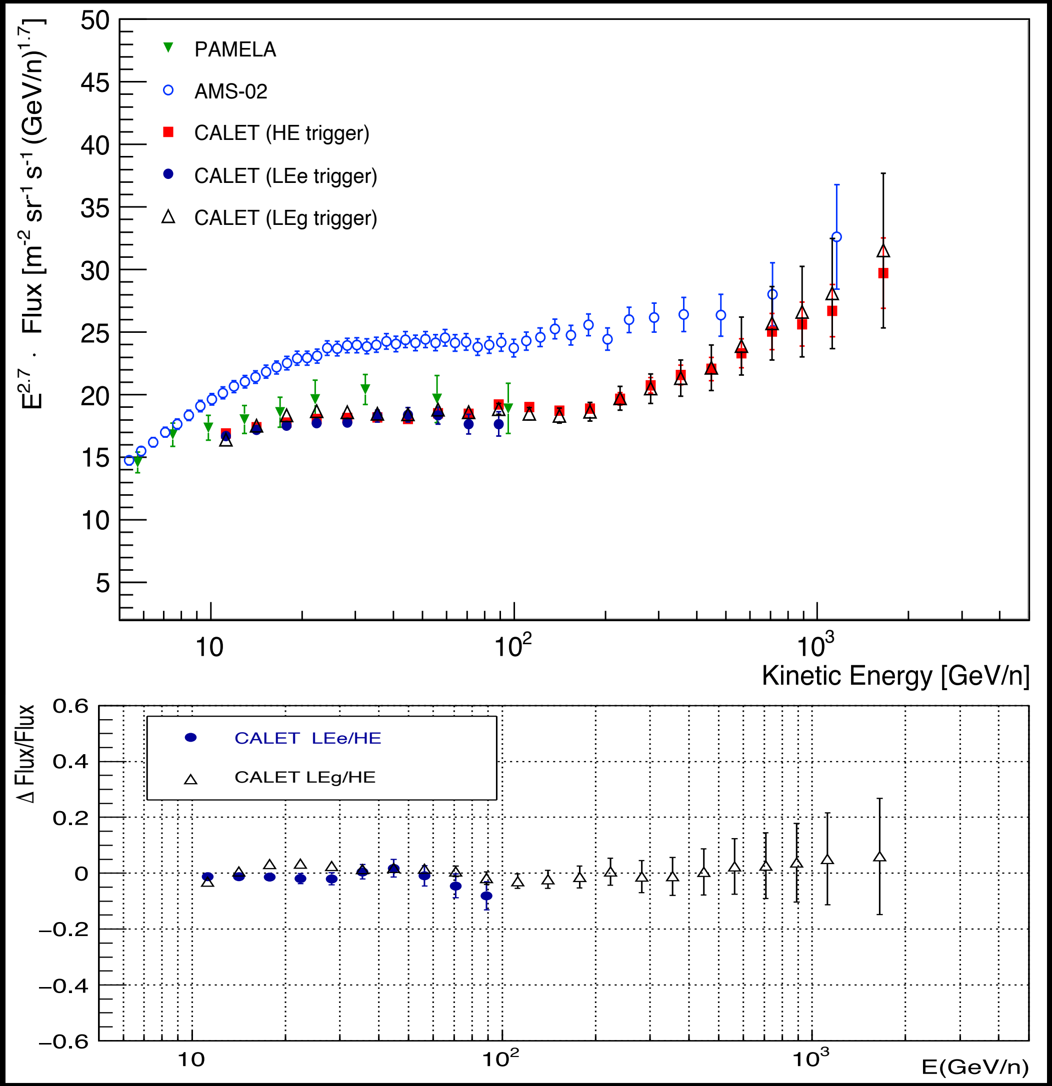

Low-energy gamma (LEg) trigger

- Coincidence of last two pairs of IMC layers (5 MIP thr.) & top TASC layer (10 MIP thr.)
- livetime ~10% of HE livetime

Low-energy electron (LEe) trigger

- same as LEg with additional coincidence of CHD & upper IMC layers (0.3 MIP thr.)
- operated at a high geomagnetic latitude
- livetime ~2% of HE livetime

The resultant fluxes using data from the different trigger modes show consistent normalization and spectral shapes.

Flux Ratios of Nickel to Primary Elements

CRD2-02

Ni ratios to He, C, O and Fe

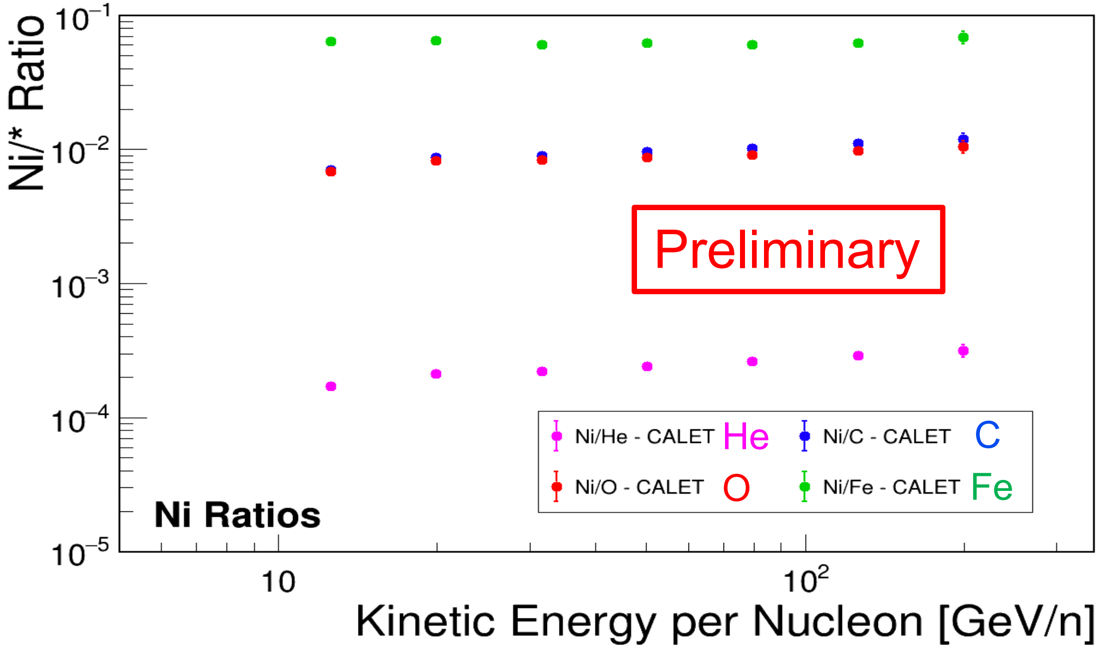

Ni ratios normalized at around 10 GeV/n

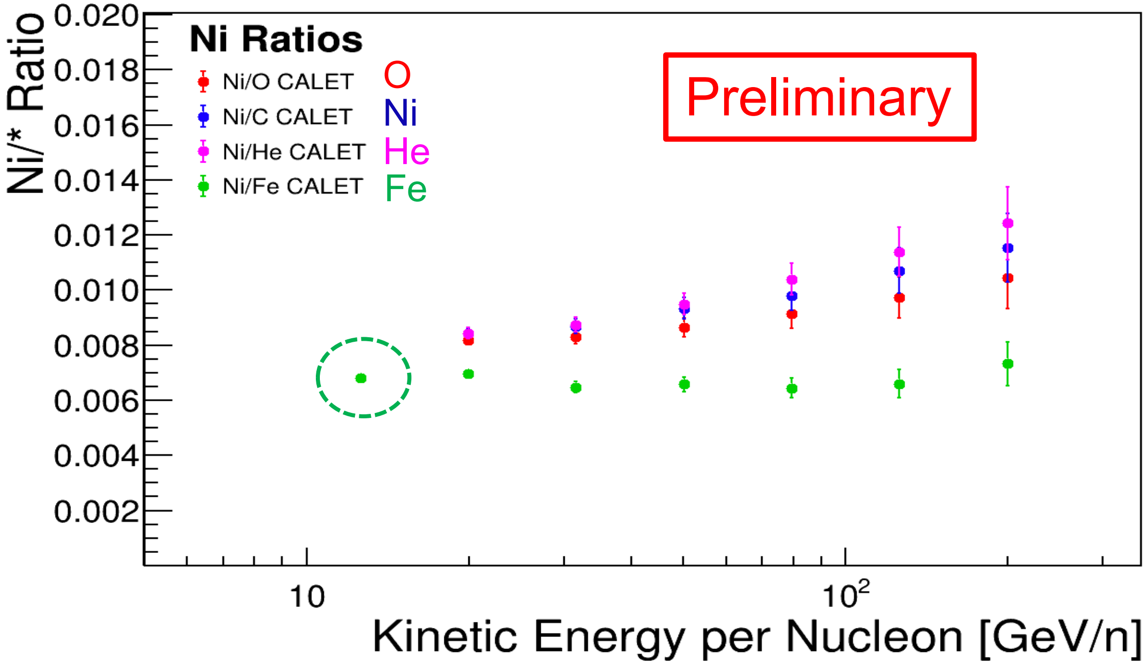

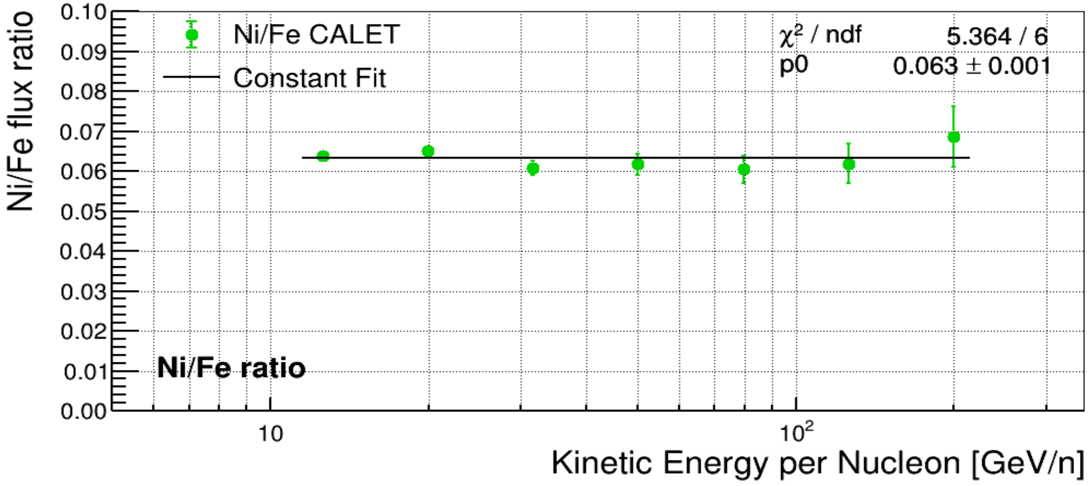

- The Ni/Fe flux ratio is constant in all the energy range thus Ni and Fe have very similar behavior in all the energy range.
- The present energy range of nickel flux does not allow to fit the Ni/* ratios with a constant above 100 GeV/n.
- At low energy the Ni/O, Ni/C, Ni/He flux ratio show an increasing trend also visible in Fe/* ratios.

CALET GeV-energy Gamma Rays

- Effective area: ~400 cm2 (>2 GeV)
- Angular resolution: < 0.2° (> 10 GeV)
- Energy resolution: ~2% (> 10 GeV)

LE-γ trigger (E > 1 GeV)

HE trigger (E > 10 GeV)

Nov 2015 – Dec 2022

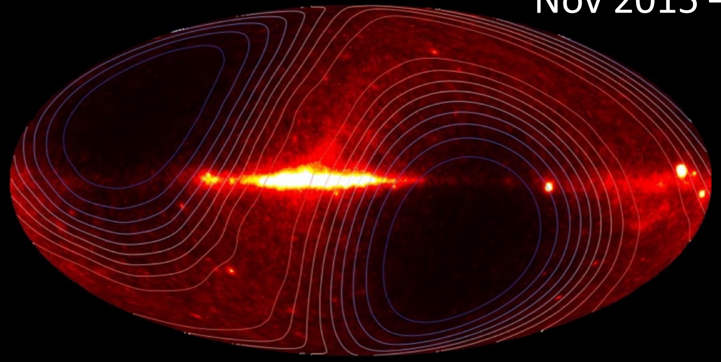

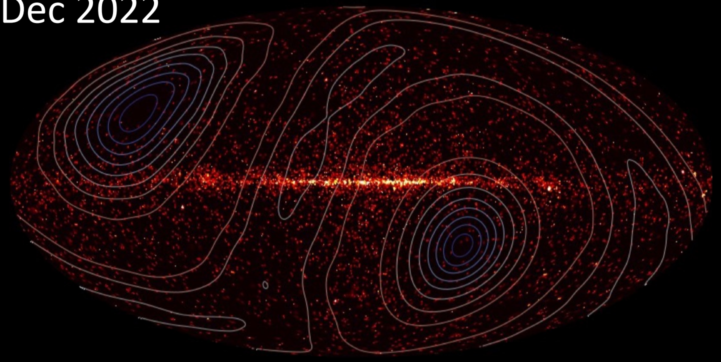

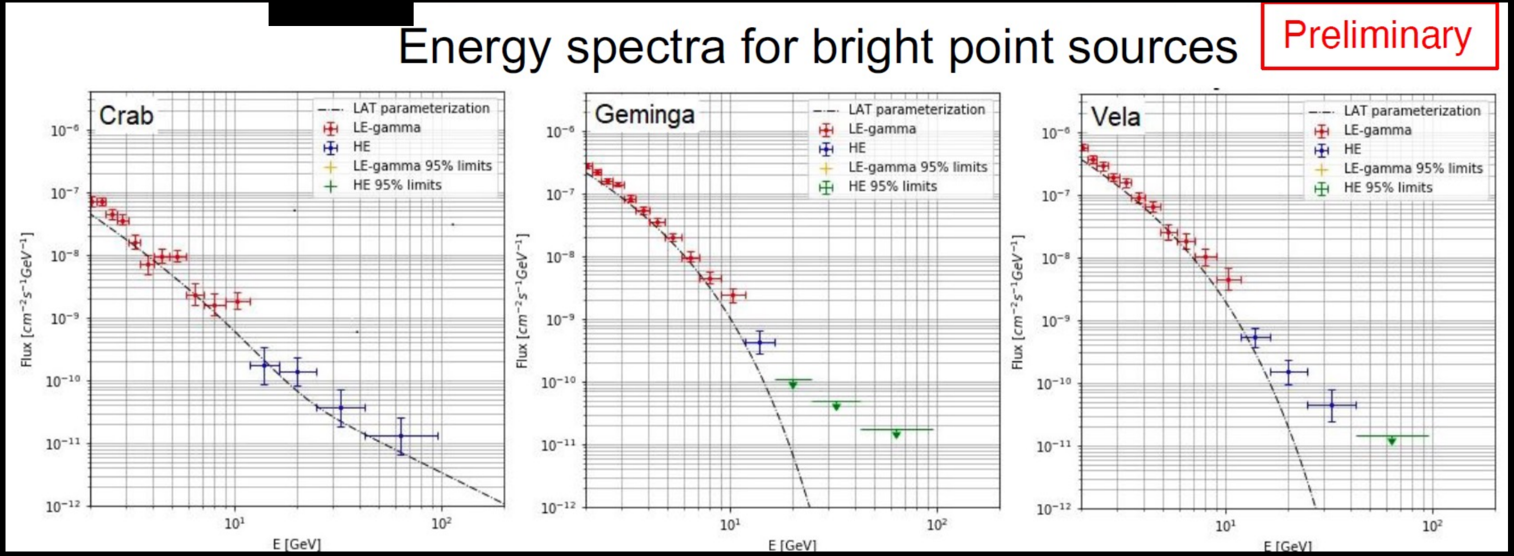

Average galactic spectra

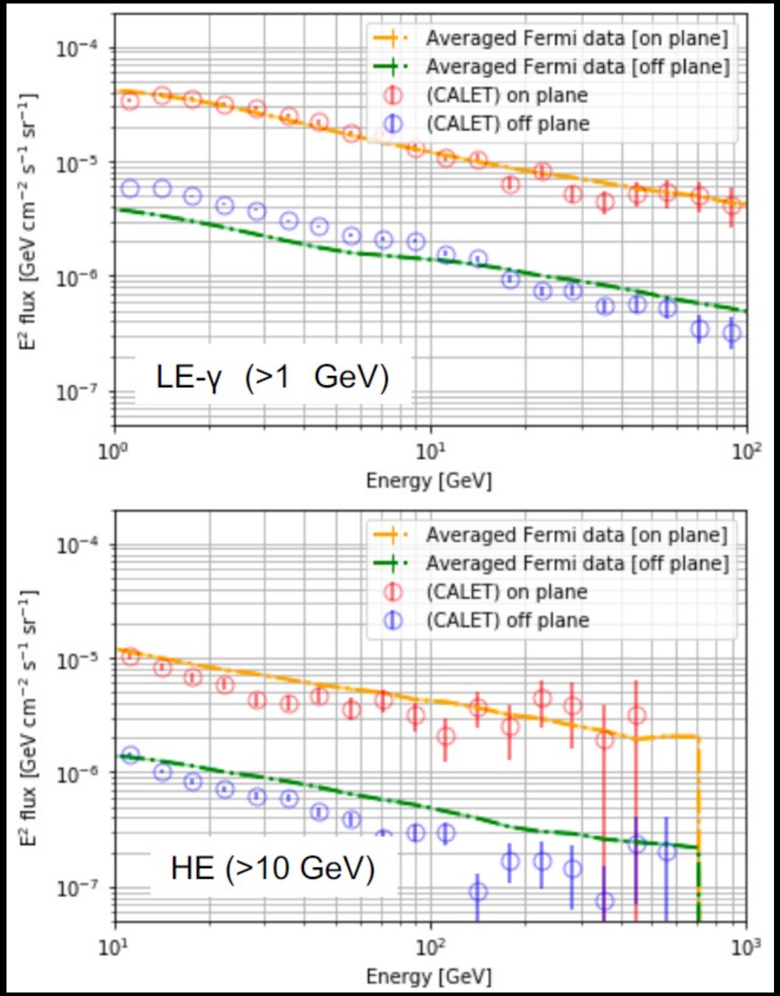

Measurements of energy spectra for point sources and diffuse structures are found to be consistent with those by Fermi-LAT.

On-plane: $|\ell| < 80° \;\&\; |b| < 8°$

Off-plane: $|b| > 10°$

CALET Gamma-ray Burst Monitor

CGBM has performed GRB observations on ISS for more than 8 years.

2015/10/05 ~ 2024/06/30
365 GRBs (onboard triggered)
Short: 46 (< 2.0 s) Long: 319

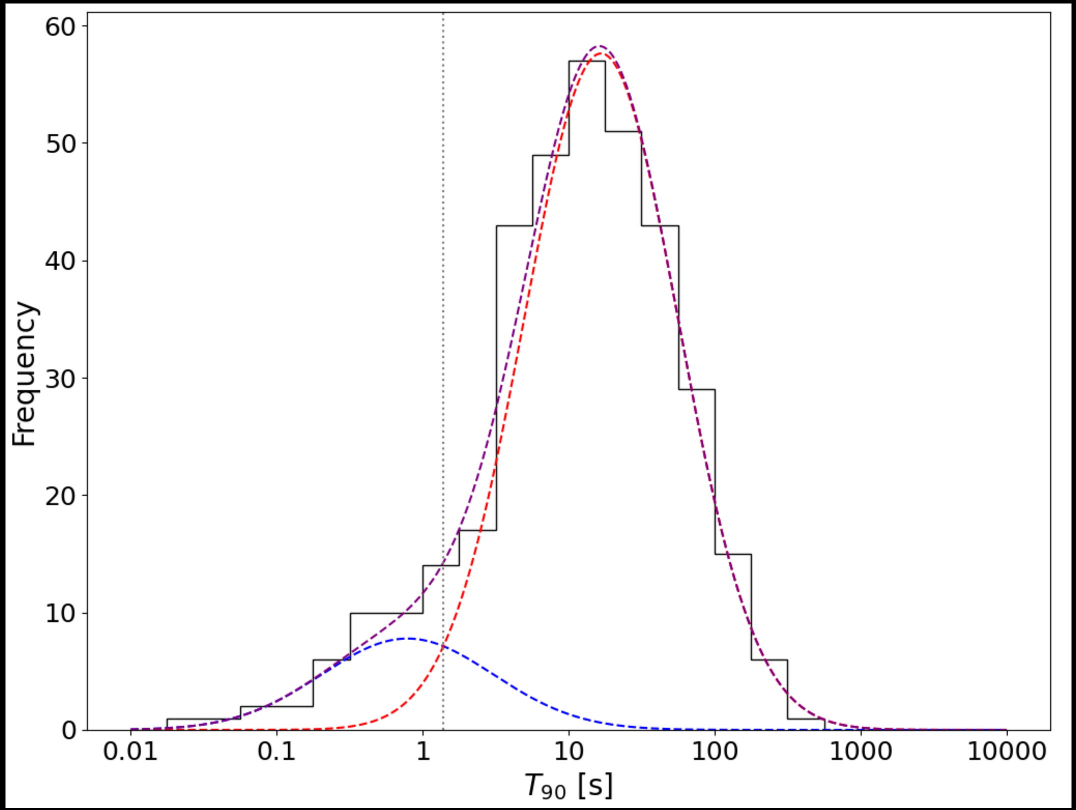

Hard X-ray Monitor
7 – 1000 keV

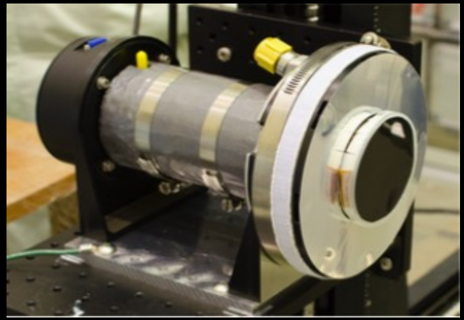

Soft Gamma-ray Monitor
40 keV – 20 MeV

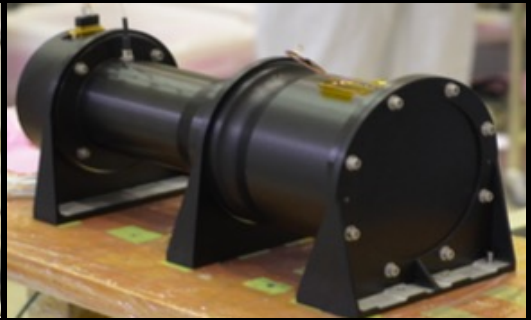

counterparts

O4a (and ER15): 85 significant events
37 : HV off
3 : Outside of the FOV
45 : (Partially) Inside of the FOV

O4b (and ER16) : 35 significant events
21 : HV off
14 : (Partially) Inside of the FOV

No candidates of counterparts so far.

Charge-sign Dependent Solar Modulation

PRL 130, 211001 (2023)

ICRC 2023 Update

Solar Modulation during Solar Cycles 24-25 Transition

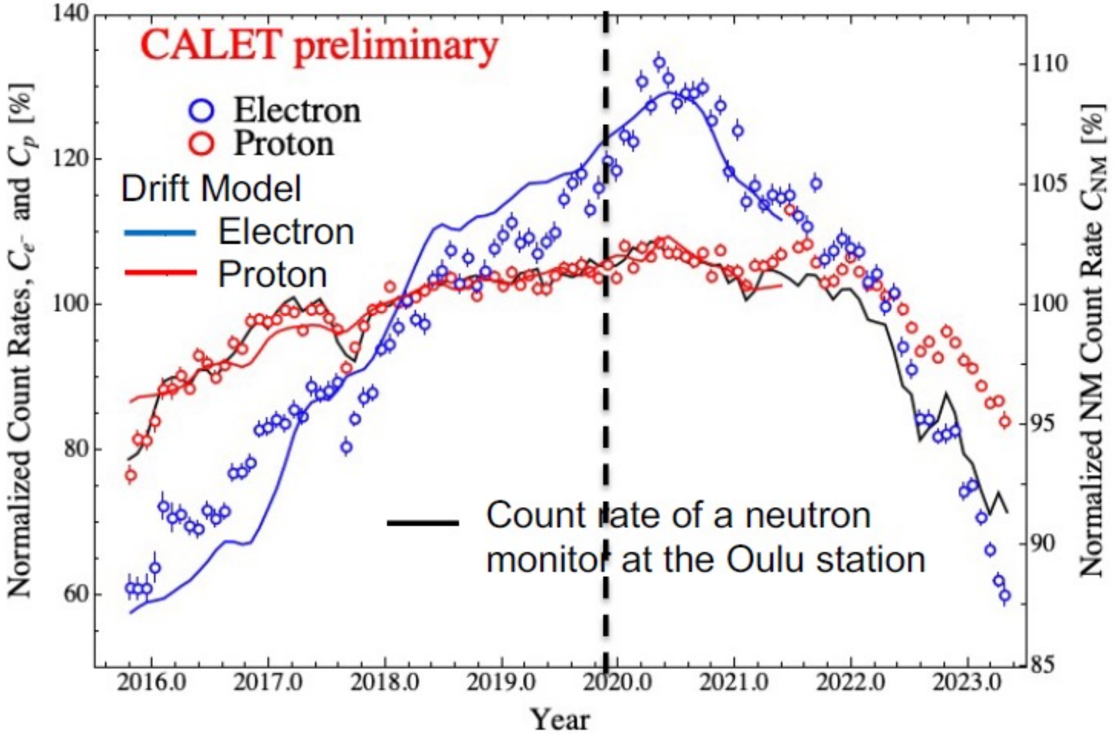

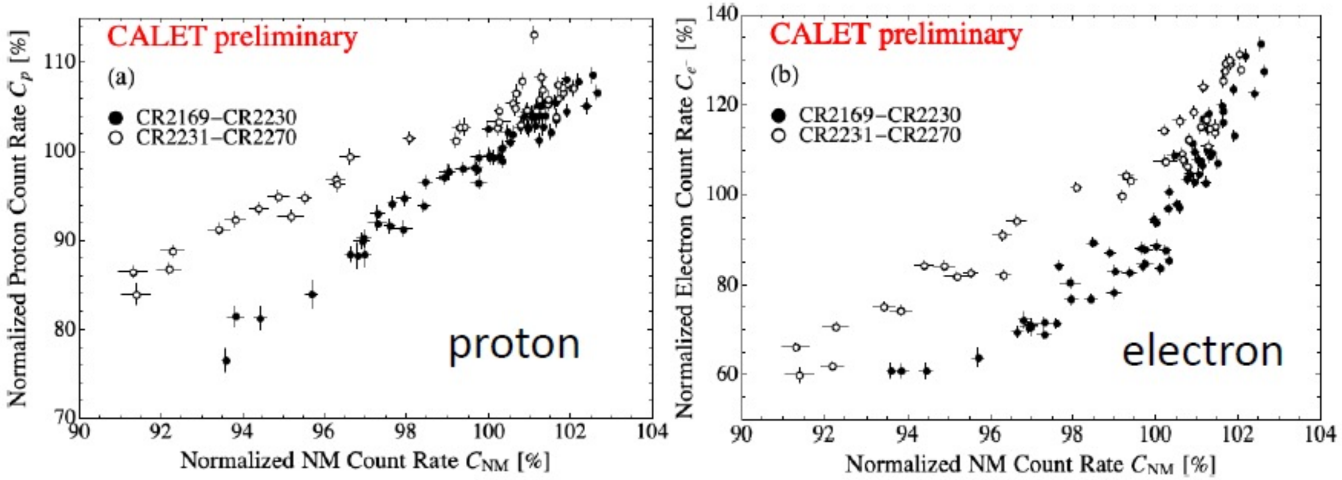

CALET proton (a) and electron (b) count rates at the average rigidity of 3.8 GV as a function of neutron monitor count rates at the Oulu station during the descending phase in the 24th solar cycle (closed circles) and the ascending phase in the 25th solar cycle (open circles).

- We have observed a clear charge-sign dependence of the solar modulation of GCRs, showing that variation amplitude of C_{e-} is much larger than that of C_p at the same average rigidity.
- We also have succeeded in reproducing variations of C_{e-} and C_p simultaneously with a numerical drift model of the solar modulation, which implies that the drift effect plays a major role in the long-term modulation of GCRs.
- We also find a clear difference between ratios, C_p/C_{NM}, during the descending phase of the 24th solar cycle and the ascending phase of the 25th solar cycle.

Space Weather Transients

- Objectives of CALET include continuous monitoring of space-weather phenomena in the LEO radiation environment, including relativistic electron precipitation (REP) from the outer Van Allen Belt

- REP drivers were investigated in magnetically conjugate observations by CALET and Van Allen Probes, showing the role of wave scattering and the contribution of EMIC-wave driven precipitation to radiation-belt losses (Bruno et al., 2021†; Blum et al., 2024‡)

CALET and Radiation Belt Science Probes (RBSP)

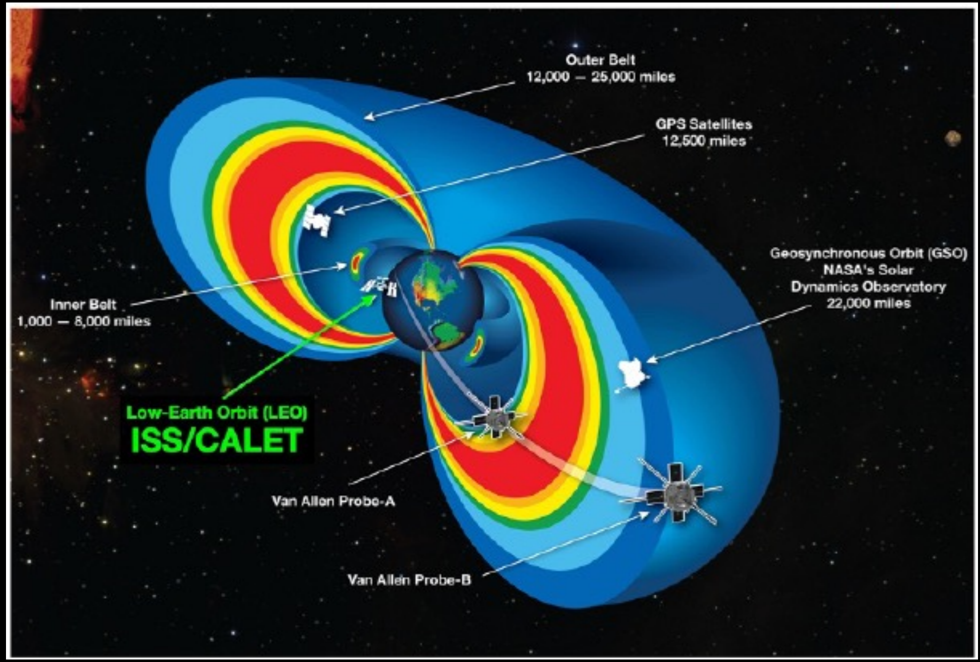

Relativistic Electron Precipitation Events with CALET

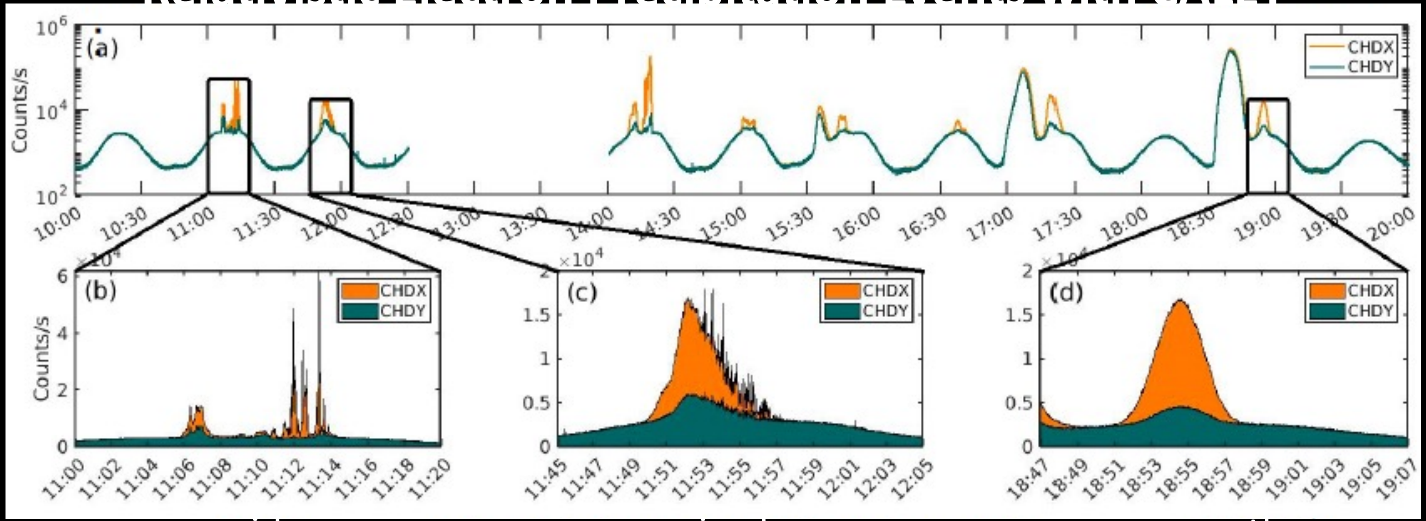

- An automated algorithm based on machine-learning techniques was implemented to identify and classify the REP events collected during >9 years of the mission (Vidal-Luengo et al, 2024a•)

- The large statistical sample allowed to investigate the contribution of REP to the radiation belt dropouts, and the correlations with solar-wind/geomagnetic drivers (Freund et al., 2024*)

- The occurrence of REP events was found to exhibit a semi-annual variation (peaking at equinoxes), in agreement with the temporal periodicity of outer-belt electron intensities (Vidal-Luengo et al, 2024b^)